Palaeogeography, Palaeoclimatology, Palaeoecology 680 (2025) 113330

Contents lists available at ScienceDirect

Palaeogeography, Palaeoclimatology, Palaeoecology

journal homepage: www.elsevier.com/locate/palaeo

Early organic carbon and nitrogen accumulation in a Pyrenean site: From rock to peat across the Late Glacial–Early Holocene transition

Teresa Vegas-Vilarrúbia [a,*], Arnau Blasco [a], Sandra Garcés-Pastor [a,b], Maarten Blaauw [c], Miguel Ángel Calero [d], Valentí Rull [e,f]

[a] Department of Evolutionary Biology, Ecology and Environmental Sciences, Universitat de Barcelona, Av. Diagonal 643, 08028 Barcelona, Spain
[b] Institute of Marine Sciences (ICM-CSIC), Pg. Marítim de la Barceloneta, 37, Ciutat Vella, 08003 Barcelona, Spain
[c] CHRONO Centre for Climate, the Environment and Chronology, School of Natural and Built Environment, Queen's University Belfast, United Kingdom
[d] Department of Geography, Universitat de Barcelona, C/ de Montalegre, 6, Ciutat Vella, 08001 Barcelona, Spain
[e] Botanic Institute of Barcelona, Spanish National Research Council (CSIC), Pg. del Midgia s/n, 08038 Barcelona, Spain
[f] Institut Català de Paleontologia Miquel Crusafont, Universitat Autònoma de Barcelona, C. de les Columnes s/n, ICTA-ICP Bld., 08193 Cerdanyola del Vallès, Spain

ARTICLE INFO

Editor: Pradeep Srivastava

Keywords:
Alpine peatbog
Carbon storage
Peatland onset
Climate change
Carbon sources
Biogeochemical markers
Diatoms

ABSTRACT

Understanding carbon-climate feedbacks during past climate transitions is critical to projecting long-term Earth system responses. Peatlands, though covering only 3–4 % of the terrestrial surface, play a disproportionate role in the global carbon cycle. Yet, Late Glacial peatlands in southern Europe remain understudied due to their rarity and fragmented records. This study provides a sub-centennial, multi-proxy reconstruction (15–10 cal kyr BP) from the Bassa Nera peat bog in the Central Pyrenees, combining total organic carbon (TOC), total nitrogen (TN), carbon accumulation rates (CAR), stable isotopes ($\delta^{13}C$, $\delta^{15}N$), diatom assemblages, and charcoal influx.

During the Oldest Dryas (GS-2 stadial), low TOC and TN suggest limited microbial activity under dry conditions. Despite climatic variability during the Bølling/Allerød (GI-1 interstadial), organic and isotopic signals remained damped. The Younger Dryas (GS-1 stadial) marks a shift, with abrupt peaks in TOC and TN (~12.8 cal kyr BP), signaling the onset of organic accumulation. Sustained peat development begins around 12.3 cal kyr BP, accelerating in the Early Holocene with increased C/N ratios, charcoal influx, and isotopic changes, indicating higher terrestrial productivity and wetter conditions. Principal Component Analysis reveals evolving organic matter sources linked to regional vegetation dynamics.

Bassa Nera is among the earliest peat-forming systems in the mountains of southern Europe, offering novel insights into long-term carbon accumulation patterns in montane settings. These findings highlight the role of early postglacial peatlands in shaping regional carbon dynamics and emphasize the need to incorporate underrepresented southern systems into global carbon and climate assessments.

1. Introduction

This study investigates the dynamics of organic carbon (TOC) and nitrogen (TN) accumulation in a Late Glacial to Early Holocene sequence spanning 15 to 10 thousand calibrated years before present (cal kyr BP), where peatlands are scarcefocus is the Bassa Nera peat bog, located on the southern side of the central Iberian Pyrenees.

Peatlands cover approximately 3–4 % of Earth's land surface (Blodau, 2002; Clymo et al., 1998) yet store nearly 30 % of global soil carbon (Gorham, 1991). Despite this, degraded peatlands contribute around 4 % of global anthropogenic greenhouse gas emissions (Ramsar, 2021; Wetlands International, 2025), as carbon is released due to moisture loss, land-use changes, and fires (Harenda et al., 2018; Ramsar, 2021). While the best-known peat carbon sinks are in northern and subarctic zones (Yu et al., 2010), less is known about peatlands at lower latitudes, which may store substantial carbon stocks and be more vulnerable to climate change due to their location near the climatic margins of peatland distribution (Treat et al., 2019). In Europe, this issue is especially pronounced in the south, where peatlands are scarce and highly fragmented (Chico et al., 2020, Tanneberger et al., 2017)

Most modern peatlands in northern latitudes formed during the Holocene (8–6 cal kyr BP), and few are older than 20 cal kyr BP (Gorham

* Corresponding author.
E-mail addresses: tvegas@ub.edu (T. Vegas-Vilarrúbia), arnaublasco@ub.edu (A. Blasco), sandragarces@ub.edu (S. Garcés-Pastor), maarten.blaauw@qub.ac.uk (M. Blaauw), miguel_angel_calero@ub.edu (M.Á. Calero), vrull@csic.es, Valenti.rull@icp.cat (V. Rull).

https://doi.org/10.1016/j.palaeo.2025.113330
Received 9 April 2025; Received in revised form 2 September 2025; Accepted 8 October 2025
Available online 15 October 2025

et al., 2007). While these systems played key roles in long-term carbon accumulation (e.g., Loisel et al., 2014, 2017), much less attention has been given to peat development during the Late Glacial—a period marked by abrupt climatic shifts and lower atmospheric CO_2 levels. This period represents the transition from glacial to interglacial conditions and is characterized by a well-defined sequence of stadial and interstadial phases, documented through the INTIMATE stratigraphy based on Greenland ice cores (Rasmussen Clausen et al., 2014).

The main climate stages include:

- GS-2.1a (Oldest Dryas), ~17–14.7 cal kyr BP;
- GI-1 (Bølling/Allerød), 14.7–12.9 cal kyr BP, subdivided into GI-1a to GI-1e;
- GS-1 (Younger Dryas), 12.9–11.7 cal kyr BP, the final Pleistocene cooling;
- Early Holocene (Greenlandian Stage), 11.7–8.2 cal kyr BP

Though terrestrial archives may exhibit slight offsets relative to ice-core records, palaeoclimate data from the Pyrenees—such as the Ostolo and Seso speleothem records—show good correlation with the INTIMATE sequence (Bernal-Wormull et al., 2021; Bartolomé et al., 2015). These records reflect the Younger Dryas and 11.4 cal kyr BP cold event, although some events, like the GI-1c1 cooling, are missing or shifted in the OST2 record.

Peat bogs require millennia to form and are influenced by long-term accumulation of organic material from autochthonous and allochthonous sources under variable hydrological and climatic regimes. Factors influencing pre-Holocene peat development include temperature, precipitation, topography, and vegetation changes. Understanding their origins is essential to reconstruct long-term carbon-climate feedbacks.

In the Iberian Peninsula, Late Glacial intervals are ideal for studying ecosystem responses to natural climate variability in the absence of significant human disturbance (Carrión et al., 2020; Oliva et al., 2019), especially in mountainous regions. The Aiguamòg River basin, located in the Pyrenees, encompasses the Bassa Nera peat bog and the nearby Ruda Valley—two key sites situated within the Aran Valley on the northern flank of the mountain range. Geomorphological and palynological evidence indicates that this basin was influenced by major Late Glacial climatic oscillations, particularly the Bølling-Allerød interstadial and the Younger Dryas stadial (Fernandes et al., 2022; Rull et al., 2023).

These marked climatic shifts are expected to be reflected in the ecological responses of wetland ecosystems in the region, particularly in terms of hydrological and vegetation dynamics. Such changes likely played a pivotal role in initiating peatland development and influencing subsequent carbon accumulation in these montane environaments. To test this hypothesis, we analysed sedimentary core PATAM12-A-14 from the Bassa Nera peat bog. This core provided the first well-dated, complete, and continuous (gap-free) Late Glacial to Early Holocene sequence (~15.2 to 10 cal kyr BP) at sub-centennial resolution from the central Iberian Pyrenees. This high-resolution archive offers a unique opportunity to trace the onset of peat accumulation and its subsequent development under varying climatic conditions. To our knowledge, no previous studies in this region have provided such a continuous and chronologically constrained record for this time interval.

To investigate the origin and temporal variability of organic matter in the peat bog, we employed a multi-proxy approach combining geochemical and biological indicators to reconstruct peatland dynamics at sub-centennial resolution. The integrated analysis of these proxies in a well-preserved peat core provides valuable insights into key processes such as organic matter decomposition, nutrient cycling, vegetation change, and hydrological variability. Nevertheless, the interpretation of these signals must consider the influence of multiple environmental and taphonomic factors (see main references in Table 1).

Our main objectives were as follows:

Table 1
Range values and references for terrestrial and aquatic sources of the carbon to nitrogen ratio (C/N) and $\delta^{13}C$ and $\delta^{15}N$ isotopes.

Biogeochemical indicators	Range values for terrestrial or aquatic sources	References
C/N ratio	4–10 aquatic source 2.6–4.3 bacterioplankton >20 terrestrial sources, C3 and C4 plants	Meyers, 1994, 2003, Wu et al., 2021; Ku et al., 2007
$\delta^{13}C$ values	Terrestrial plants −32 ‰ to −22 ‰ Aquatic source (plankton) -22 ‰ to −18 ‰ Typical C_3 plants: −24 ‰ to −30 ‰. Typical C_4plants: −9 ‰ to −16 ‰.	Kendall et al., 2008; Pu et al., 2023; Ku et al., 2007 Kohn, 2010; Diefendorf et al., 2010
$\delta^{15}N$	-	Craine et al., 2015; Thornton and McManus,1994. Ku et al., 2007

- To trace the onset of peat formation at Bassa Nera and to reconstruct carbon and nitrogen fluxes and accumulations between 15 and 10 cal kyr BP during the Late Glacial period at subcentennial-scale resolution, with special attention on intervals of abrupt climate change.
- To identify the potential sources of carbon and nitrogen contributing to peat bog development over time, using geochemical indicators and available palaeoecological evidence.
- To assess the influence of climatic variability patterns on carbon and nitrogen ccumulation dynamics, using independent paleoclimate records

We compared our results with those from other mountain peatland records in southern Europe that share similar climatic and biogeographic contexts.

Given the role of peatlands as major carbon sinks, understanding their development during the Late Glacial period is critical for informing strategies aimed at enhancing carbon sequestration in the context of climate mitigation. Reconstructing their early dynamics provides a valuable long-term perspective on carbon storage potential under changing climatic conditions. In parallel, this knowledge offers a historical baseline for assessing the original functioning of peatland ecosystems and their ecological resilience. Such insights can contribute to the design of more effective conservation and restoration initiatives adapted to future climate scenarios.

2. Materials and methods

2.1. Regional settings

Currently, Bassa Nera is a small pond that is approximately 100 m long, 60 m wide, and 5 m deep. It is located in a small depression known as Pletiu dera Muntanheta, situated in the headwaters of the Aiguamòg valley (upper Garona basin), at 42°38′17″ N and 0°55′27″ E, with an elevation of 1890 m (Fig. 1). The origin of the Aiguamòg River lies in the glacial lakes nestled in the Colomers cirque. During its course, the river receives contributions from three tributaries: the arriu dera Montanheta, the Barranc des Pletius, and the barranc deth riu Medèr. Eventually, the river is impounded to create the Aiguamog reservoir and, downstream, it merges with the Garonne River near Tredós. The Upper Garonne Basin represents as the most significant glacial system that prevailed in the Pyrenees during the last glaciation (Termination-1, T-1). Throughout this period of glacial recession, the oscillations in glacier advancement and retreat substantially moulded the geomorphological features of the region. Nevertheless, the precise chronology of the T-1 glacial oscillations on the northern slopes of the Central Pyrenees remains a topic of uncertainty, with limited data. However, in the adjacent Ruda Valley, an

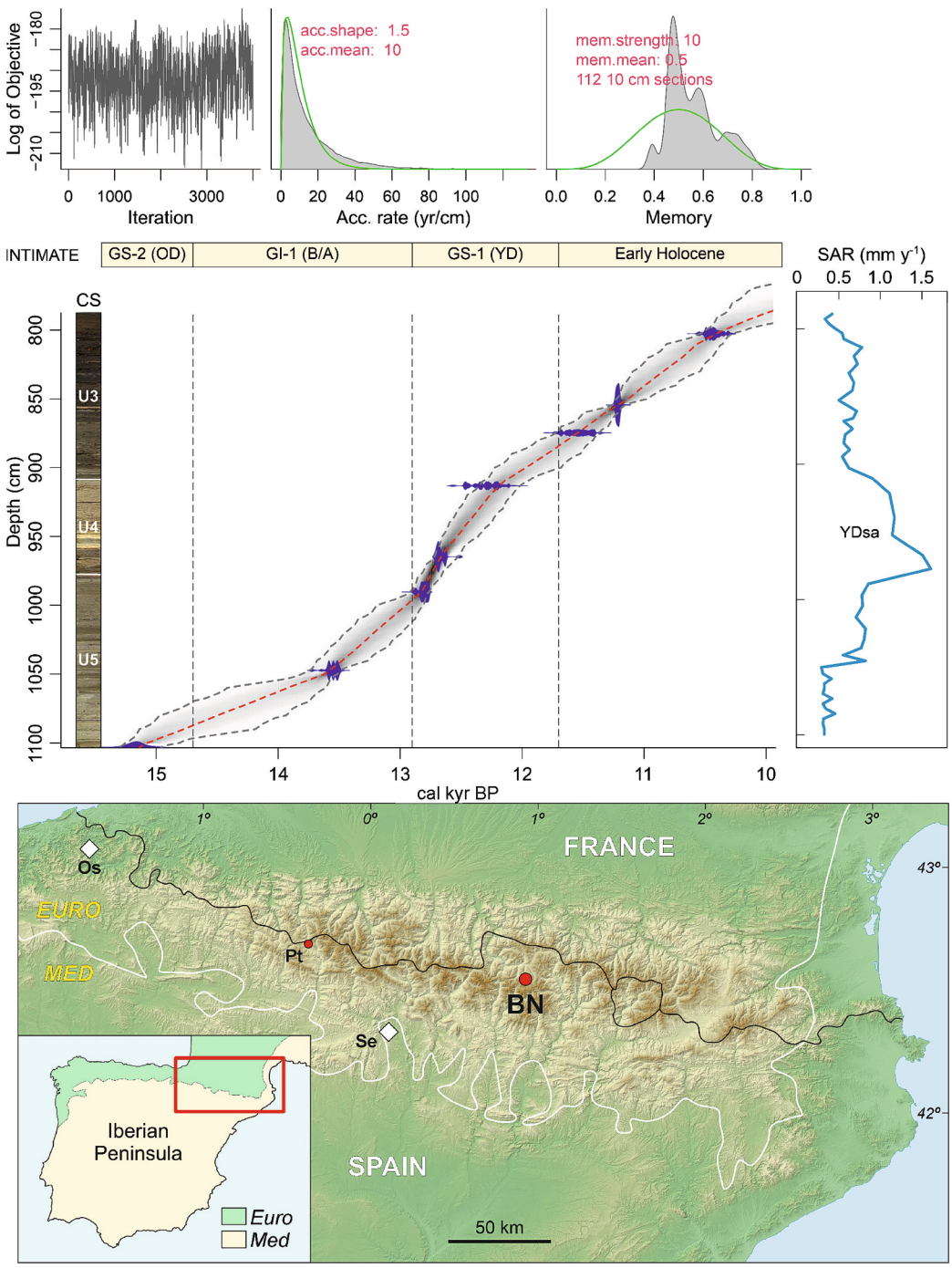

Fig. 1. A: Lithology, Bacon age–depth model, and sediment accumulation rates for core PATAM12-A14. Radiocarbon-dated samples are shown in blue; the model mean is indicated by a red dashed line, with 95 % confidence intervals in grey. INTIMATE stratigraphy is included for reference. B: Map of the Iberian Peninsula showing the study site (red rectangle) and the Eurosiberian (green) and Mediterranean (pale yellow) biogeographical regions. C: Pyrenean mountain range with Bassa Nera (BN) and other Late Glacial coring sites: Ba, Balcère; Bu, Búbal; Fr, Freyxinède; Go, Gourg-Nègre; La, Laurenti; Ma, Marboré; Pr, Portalet; Pt, La Pouretère; Ra, Racou; Tr, Tramacastilla. (Modified from Rull et al., 2023). (For interpretation of the references to colour in this figure legend, the reader is referred to the web version of this article.)

area housing a sequence of moraines and polished surfaces, Fernandes et al. (2022) conducted a series of geomorphological observations and dating analyses. These efforts facilitated the reconstruction of an exhaustive chronology of Pyrenean glacial oscillations spanning from GI-2 (B/A) to the GS-1 (YD). These two climatic episodes were marked by abrupt transitions, and thus, they hold considerable scientific interest in the context of ecosystem responses to sudden climatic alterations, similar to those occurring in the present day. The BN peat bog is in the Eurosiberian climate region and hence is influenced by moist westerly winds from the Atlantic Ocean. It is characterized by cool to temperate conditions with high precipitation and moderate temperatures. The nearest meteorological station, Port de la Bonaigua, is situated approximately 6 km to the northeast at an elevation of 2072 m, which is 182 m above Bassa Nera. Over the period from 1990– to 2020, the annual average temperature was recorded at 3.34 °C, and the total annual precipitation reached 1218 mm. Notably, the lowest temperatures,

ranging between −2.9 and − 3.2 °C, are typically observed in January and February, whereas the highest temperatures, reaching 11.6 °C, are experienced in July and August. The precipitation exhibits a bimodal pattern, with peak values of 131–137 mm occurring in May and November, and the lowest values of 70–79 mm occurring in February and July. Currently, the BN is surrounded by a complex of wetlands and peatlands dominated by *Sphagnum* sp. and *Carex lasiocarpa*, with an abundance of other elements such as *Molinia caerulea, Drosera longifolia, Menyanthes trifoliata* and *Parnasia palustris*. Regionally, it is approximately 400–500 below the subalpine black pine (*Pinus ucinata*) treeline (Carrillo et al., 2008; Garcés-Pastor et al., 2017). Our previous limnological assessments during the ice-free seasons of 2014, 2020 and 2021 revealed a moderately acidic, low-conductivity and nutrient -rich aquatic environment with relatively low oxygen levels in the bottom layers (Vegas-Vilarrúbia et al., 2024). These conditions are characteristic of many peat bogs (Joosten and Convention on Wetlands, 2021).

2.2. Coring and dating

The Bassa Nera core PATAM12-A14 used in this study was retrieved in July 2014 with a 50-mm diameter Livingstone corer (Fig. 1). This core consisted of 10 drives (D1 to D10) with a total length of 845 cm (1102 cm once corrected for compression). This study focused on the basal sequence (drives D7 to D9), which contains the Late Glacial-Early Holocene (LGEH) interval with no apparent gaps. Eight samples for radiocarbon dating were taken in this interval and subjected to acid/base digestion (KOH, HCl, HF) to eliminate the rejuvenating effect of eventual incorporation of younger plant material and/or humic acids percolating through the peat profile. AMS radiocarbon dating was conducted at the Radiocarbon Laboratory, Université Laval (Canada), and the results, along with the corresponding age model, were previously published (Rull et al., 2023). A modified summary of the radiocarbon ages (14C yr BP), including 1σ analytical errors (± years), and calibrated ages (Cal yr BP) as 95 % confidence intervals (2σ), is presented in Table S1 (Supplementary material). Calibration was carried out using CALIB 8.2 and IntCal 20 (Reimer et al., 2020). The Bayesian age–depth model (Fig. 1) was constructed using the BACON software (Blaauw and Christen, 2011). The studied interval contained a continuous LG-EH sequence spanning approximately 5000 years, from 15.3 to 10.3 cal kyr BP. This sequence included the GS-2, GI-1, GS-1 stages and part of EH warming. The average sediment accumulation rate was 0.63 mm/yr, but it varied, with rates of 0.29–0.82 mm/yr in Units 3 and 5 and higher rates in Unit 4 (0.90–1.60 mm/yr). This acceleration occurred during the early GS-1 (12.8–12.3 cal kyr BP). In this study, the temporal resolutions of the different records, i.e. carbon, nitrogen, diatoms and palynomorphs (see section 3.4) is centennial and the respective samples were taken from the same sediment core and at equivalent depths. Given the confirmed strong agreement between pollen zones and the INTIMATE event stratigraphy (Rull et al., 2023), we employed the same climatic framework.

2.3. Carbon, nitrogen and isotopic analyses

We used a suite of biogeochemical indicators, including measures of total organic carbon (TOC), total nitrogen (TN), total carbon to nitrogen molar ratios (C/N), carbon accumulation rates (CAR), nitrogen accumulation rates (NAR), carbon ($\delta^{13}C$), ($\delta^{15}N$) nitrogen isotopic ratios and diatoms species are examined within the sediment samples. One hundred sediment samples were extracted from the core (PATAM12-A14) and weighed. A known volume of each sample ($1 cm^3$) was desiccated in an oven, weighed and subjected to analysis at the Gas Chromatography–Mass Spectrometry Unit of the Scientific and Technological Centres at the University of Barcelona. Prior to analysis, the samples were treated with 30 % diluted HCl to distinguish between organic and inorganic C. The employed methodology involved elemental analysis coupled with isotope ratio mass spectrometry (EA-IRMS) using a Flash IRMS-Δ V Advantage instrument from ThermoFisher Scientific. The samples underwent the same preparatory procedures as those employed in organic elemental analysis, with a notable distinction being that the gases generated during sample combustion (N_2 and CO_2) were not purged but instead directed into an IRMS system. This coupling with IRMS facilitated the determination of isotopic compositions, specifically $\delta^{15}N$ and $\delta^{13}C$. Isotopic values were reported in δ per mil (‰) units and were calculated in accordance with internationally adopted standards. Notably, the $\delta^{15}N$ values were expressed relative to the atmospheric air composition ($\delta^{15}N_{air}$), whereas $\delta^{13}C$ values were reported relative to the $\delta^{13}C$ composition of the Pee Dee Belemnite (PDB) standard, which originated from the Pee Dee Formation in the USA. The interpretation of the $\delta^{15}N$ and $\delta^{14}C$ isotopes was carried out using widely utilized and published reference values available in various bibliographic sources (Table 1).

The accumulation rates of organic carbon (C) and nitrogen (N) were derived using the methodologies outlined in previous studies (Lähteenoja et al., 2012; Tolonen and Turunen, 2006). The computations involved the integration of various parameters, including carbon and nitrogen concentrations, multiple calibrated ages and measurements of dry bulk density. This analytical approach is grounded in the utilization of raw data, ensuring a comprehensive and accurate assessment of the accumulation rates across the specified depth intervals. Carbon accumulation rates or influx ($g\ m^{-2}\ yr^{-1}$), were determined using the following equation (Lähteenoja et al., 2012; Tolonen and Turunen, 2006), based on the raw data that included the calibrated ages derived from the age–depth model model (Rull et al., 2023):

$$CAR = (r/1000) \times d \times c$$

Here, *CAR* represents the C accumulation rate ($g \times m^{-2} \times yr^{-1}$), where r is the annual sediment accumulation rate ($mm \times yr^{-1}$), d is the dry bulk density ($g \times m^{-3}$) and c is the concentration or content (g C × g^{-1} dry weight sed). The same equation was applied to compute the N accumulation rates (NAR, $g\ m^{-2}\ yr^{-1}$). The carbon–nitrogen atomic ratio (C/N) was computed to determine variations in the proportion of carbon relative to nitrogen in the sediment.

2.4. Diatom analyses

Fifty-one sediment samples were analysed for diatoms. In the present study, the temporal resolution of the diatom records and the C and N records were centennial. Both studies acquired samples from the same sediment core and at equivalent depths. One gram of moist sediment was initially weighed and subsequently dried in an oven at 40 °C for 12 h. Next, 0.1 g of the dried sediment was weighed and digested with hydrogen peroxide (30 %) to remove the organic matter. The treated samples were then mounted with Naphrax (refractive index = 1.7). To estimate the diatom concentration, a known quantity of microspheres was introduced. A minimum of 500 diatom valves were counted and identified, employing a Polyvar microscope set at 1000× magnification, striving to attain the highest possible taxonomic resolution as per the techniques outlined by Krammer and Lange-Bertalot (1999a, 1999b, 2004a, 2004b). Several indices have been computed, including the centric/pennate diatom index (C/P), which serves as an indicator of the relative prevalence of planktonic and benthic habitats (Vegas-Vilarrúbia et al., 2024). Additionally, the chrysophyte/diatom index (Cr/D) provides a quick assessment of lake-level fluctuations (Rivera-Rondón and Catalan, 2017). Autoecological investigations were conducted on the most representative taxa.

A diagram depicting the most prevalent diatom genera was generated using Psimpoll 4.27 software, which was designed for the graphic and statistical analysis of palaeoecological data (Bennett, 1996). Statistically significant zones of taxa with abundances exceeding 3 % were determined using the “Optimal Splitting by Information Content” method, as outlined by Bennett (2002). Section 2 offers a concise summary of the results obtained up to the present date.

2.5. Palynological records

To relate variations in C and N indicators with climate change indicators and available carbon sources, well-documented environmental data were extracted from a previous study at de Bassa Nera for the same interval (Rull et al., 2023), which presented the first continuous Late Glacial-Early Holocene (LGEH) pollen record for the Iberian Pyrenees and assessed relationships among vegetation shifts, climatic changes and fires. To investigate the local and regional vegetation as likely sources of organic matter to the Bassa near sediments, in this study we compared our data with the best represented taxa and chose the following: 1) sum of pollen abundances of pine, deciduous forests and herbs; 2) algae remains and fungi spores; 3) the best-portrayed charcoal particles representing regional fires, as they count as potentially significant global carbon sinks in peat (Mooney and Tinner, 2010; Turney et al., 2006).

Hence, we have summarized best represented palynological taxa during the targeted period (Fig. 2) according to Rull et al. (2023). The four distinct vegetation types included conifer and deciduous forests (F1, F2) and two open vegetation types (O1, O2) lacking modern analogues. O1 and O2 were dominated by *Artemisia*-Poaceae and *Saxifraga*-Cichorioideae, respectively. Forests prevailed during interstadial phases (B/A and EH), whereas O1 prevailed during stadials (OD and YD), and O2 only in the first half of the Younger Dryas. An unexpected discovery was the occurrence of wet climates during the Younger Dryas, substantiated by a notable increase in the abundance of algae remains. This finding aligns with a trend towards increased precipitation indicated by Seso's cave speleothem records (Fig. 2). The temporal resolutions of the selected palynological records, along with the C and N variables in the present study, are centennial. Both studies acquired samples from the same sediment core and at equivalent depths.

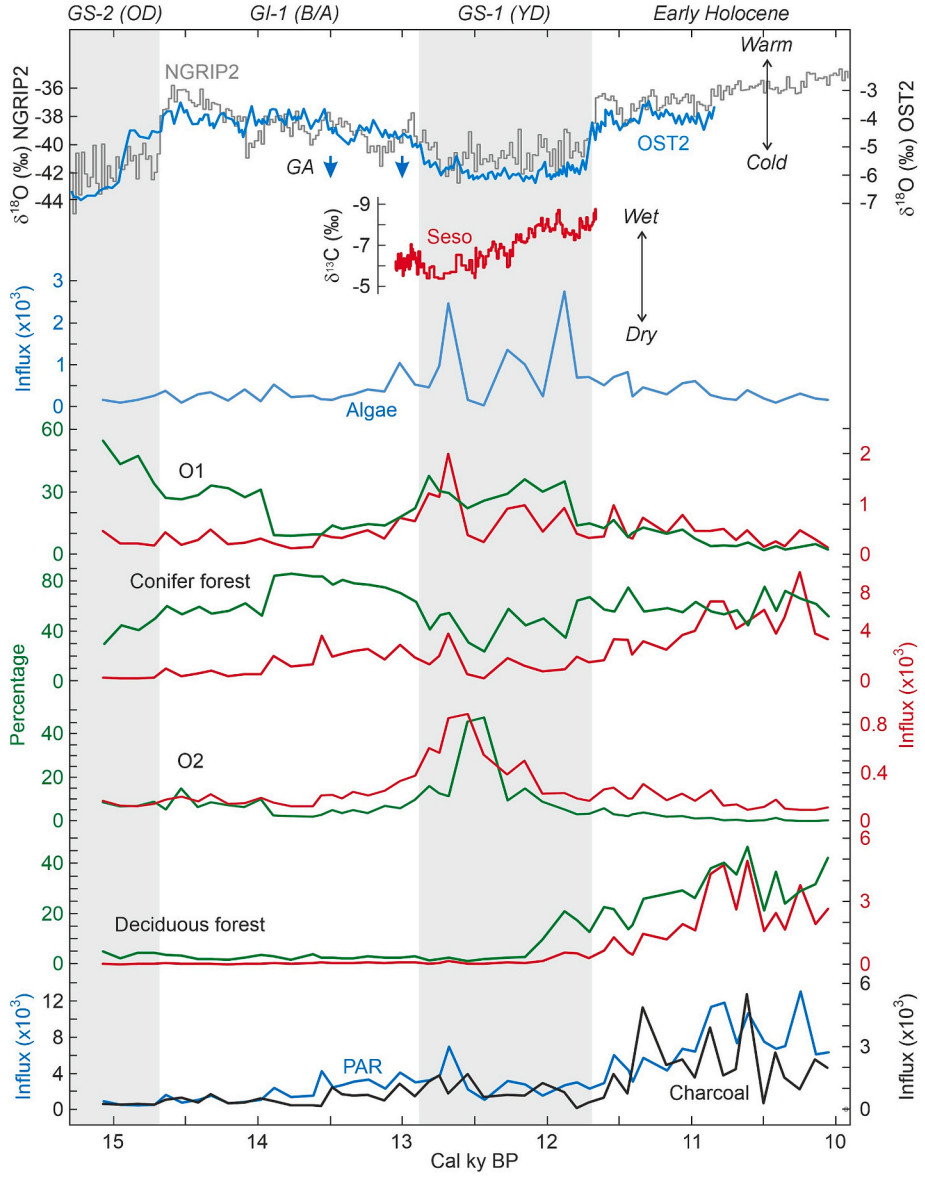

Fig. 2. The Late Glacial–Early Holocene stratigraphy from the Greenland NGRIP2 ice core (Rasmussen Clausen et al., 2014) is compared with speleothem records from Oslo cave (OST2) in the western Pyrenees (Bernal-Wormull et al., 2021) and Seso cave in the central Pyrenees (Bartolomé et al., 2015) Glacier dynamics in the Ruda valley (Fernandes et al., 2022) are also included, with GA indicating glacier advance and OD denoting the Oldest Dryas. Pollen assemblages are compared with temperature, moisture, and fire proxies, where O1 and O2 indicate non-forested vegetation types. Pollen assemblages are displayed as both percentages and influx units (grains cm^{-2} y^{-1}), organized chronologically by their respective peak values. GA indicates glacier advances in the adjacent Ruda Valley, PAR indicates pollen accumulation rates.

2.6. Statistical analyses

Similar samples were grouped by creating a dendrogram based on stratigraphically constrained hierarchical clustering and the Euclidean distance method. Concurrently, we applied Principal Component Analysis (PCA), a linear dimensionality reduction method (Legendre and Legendre, 2012), to condense biogeochemical and environmental related variables into a few components that capture the main patterns of variation. The data were analysed using Microsoft Excel spreadsheets (version 2019), and the Palaeontological Statistics Software Package for Education and Data Analysis (PAST, Hammer et al., 2001).

3. Results

3.1. Elemental and isotopic C and N analyses

The averages, standard errors and ranges of each biogeochemical variable ($n = 96$) are shown in Table 2, and the corresponding time series are displayed in Figs. 4 and 5. To extract valuable insights from the acquired data, the sediment samples were grouped together based on the similarity of their biogeochemical variables. A dendrogram was created using stratigraphically constrained hierarchical clustering and the Euclidean distance method (Fig. 3). The resulting groups delimited six stratigraphically differentiated zones (Z1–Z6) along the core. Next, we describe the values and variations in each variable and zone, from approximately 15.0 to 10.2 cal kyr. BP (Table 2, Figs. 4 and 5).

3.1.1. Zone 1: eighteen samples, 1100–1068 cm depth, c. 15.0–14.1 cal kyr BP

This zone comprises part of the OD and represents the first abrupt warming of the B/A recorded by 14.7 cal kyr BP. During this period, all the carbon indicators and the C/N ratios were fairly low, and the relatively stable values were compatible with very poor biological activity. TN and NAR slightly fluctuated, and $\delta^{15}N$ varied relatively more, with values close to 0‰. There was a small influx of charcoal particles.

3.1.2. Zone 2: eighteen samples; 1066–1026 cm depth, c. 14.0–13.3 cal kyr BP

This zone is included in a very variable phase of the B/A interstadial. TOC and TN and their respective accumulation rates showed higher and more variable values, denoting some synchrony in their fluctuations with remarkable minima towards 13.5 cal kyr BP. The C/N values remained similar to those in the previous zone but also presented a minimum at approximately 13.5 cal kyr BP. The $\delta^{13}C$ and $\delta^{15}N$ values fluctuated more intensely than those in Zone 1, and the fluctuations in the TOC, TN, CAR and NAR values appeared to be in the opposite directions. These simultaneous changes at approximately 13.5 cal y BP coincided with an increasing trend in charcoal particle flux into the sediment.

3.1.3. Zone 3: fifteen samples, 1022–952 cm depth, c. 13.2–12.5 cal kyr BP

This zone comprises the transition to and the first half of the YD cold reversal. Abrupt and intense peaks in CAR and NAR and in $\delta^{13}C$ and $\delta^{15}N$ occurred at approximately 12.8 cal kyr. BP followed by a rapid recovery to former values at approximately 12.5 cal kyr BP. In fact, visually discernible organic matter began to appear in the sediment starting at 12.7 cal kyr BP (979 mm). Remarkably, the C/N ratio reached its lowest value in the entire record at approximately 12.5 cal kyr. BP. In contrast, the TOC and TN contents were similar to those observed in the preceding zone.

3.1.4. Zone 4: sixteen samples, 946–878 cm depth, c. 12.5–11.6 cal kyr BP

This zone encompasses the second half of the YD cold reversal extending to its termination (11.7 cal kyr BP) and the first years of transition to the Holocene epoch. TOC and TN contents in the top of Zone 3 exhibited smaller fluctuations and a slight increasing trend. CAR, NAR and $\delta^{15}N$ were more stable, whereas $\delta^{13}C$ still varied greatly and presented more negative values. C/N recovered to values prior to the minimum observed in the first stages of the YD. The number of charcoal particles slightly decreased.

3.1.5. Zone 5: nineteen samples, 876–820 cm depth, c. 11.6–10.7 cal kyr BP

This zone represents the onset of the EH. There were noteworthy increases in the TOC and TN contents, recoveries in CAR and NAR and slight increases in the C/N ratios. Simultaneously, the $\delta^{13}C$ values exhibited a marked shift towards more negative values, whereas the $\delta^{15}N$ values decreased slightly. Notably, charcoal influxes displayed unprecedentedly high peaks and variations.

3.1.6. Zone 6: nine samples, 817–796 cm depth, c. 10.6–10.2 cal kyr BP

The TOC, TN and C/N values increased, whereas CAR, NAR and charcoal seemed to maintain the same variation patterns as those in Zone 5. $\delta^{13}C$ reached its minimum value across the entire record, and $\delta^{15}N$ displayed fewer fluctuations than ever before.

Table 2
Averages, standard errors and ranges of each biogeochemical variable and zone.

		TOC content	TN content	TOC influx	TN influx	C/N	δ13C	δ15N
		mg /mg DW sed	mg /mg DW sed	g· m^{-2} ·yr^{-1}	g· m^{-2} ·yr^{-1}		‰	‰
ZONE 1 ($n = 17$)	MEAN	**0.020**	**0.002**	**0.032**	**0.003**	**13.1**	**−24.7**	**−0.268**
15.0–14.2 kyr	SE	0.002	0.000	0.004	0.000	0.123	0.156	0.151
	Range	0.011 to 0.0486	0.001 to 0.004	0 to 0.08	0.002 to 0.007	12.2 to 14.2	−25.9 to-23.4	−1.40 to 0.83
ZONE 2 ($n = 18$)	MEAN	**0.029**	**0.002**	**0.075**	**0.006**	**13.7**	**−26.4**	**−0.656**
14.1–13.3 kyr	SE	0.004	0.000	0.013	0.001	0.183	0.395	0.365
	Range	0.007 to 0.056	0.000 to 0.003	0.011 to 0.226	0.001 to 0.02	11.9 to 14.9	−29.2 to −23.7	−3.26 to 2.05
ZONE 3 ($n = 15$)	MEAN	**0.038**	**0.003**	**0.189**	**0.015**	**13.9**	**−25.8**	**0.844**
13.2–12.6 kyr	SE	0.004	0.000	0.030	0.003	0.459	0.500	0.419
	Range	0.01 to 0.068	0.001 to 0.005	0.07 to 0.482	0.003 to 0.0411	7.9 to 15.3	−29.1 to-21.4	−0.82 to 4.58
ZONE 4 ($n = 16$)	MEAN	**0.065**	**0.005**	**0.136**	**0.012**	**14.2**	**−26.2**	**−0.446**
12.5–11.6 kyr	SE	0.004	0.000	0.013	0.001	0.157	0.698	0.224
	Range	0.039 to 0.089	0.003 to 0.007	0.018 to 0.254	0.007 to 0.023	13.0 to 15.3	−30.8 to-20.7	−2.98 to 0.08
ZONE 5 ($n = 19$)	MEAN	**0.149**	**0.011**	**0.017**	**0.014**	**16.3**	**−32.2**	−1.51
11.5–10.7 kyr	SE	0.012	0.001	0.006	0.001	0.307	0.522	0.16
	Range	0.04 to 0.24	0.003 to 0.015	0.078 to 0.371	0.007 to 0.02	13.9 to 19.8	−35.6 to-26.7	−2.24 to −0.45
ZONE 6 (=9)	MEAN	**0.197**	**0.013**	**0.255**	**0.015**	**18.2**	**−29.2**	**−1.86**
10.6–10.3 kyr	SE	0.004	0.000	0.023	0.002	0.283	0.945	0.110
	Range	0.176 to 0.214	0.012 to 0.013	0.171 to 0.339	0.009 to 0.021	16.9 to 19.5	−35.1 to −26.4	−1.93 to −1.54

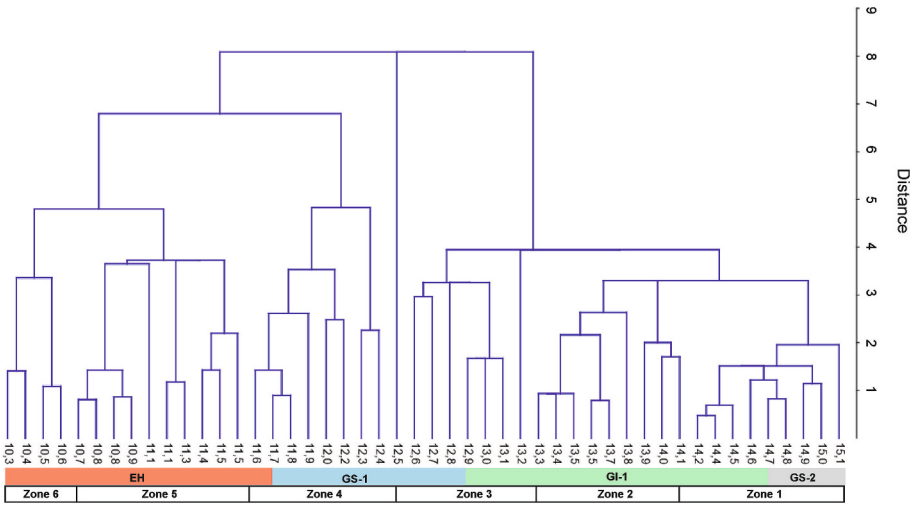

Fig. 3. Dendrogram based on biogeochemical data using stratigraphically constrained clustering and Euclidean distance. Z1-Z6: Six stratigraphic zones identified along the core. GS-2 (OD); GI-1 (B/A), GS-1 (YD).

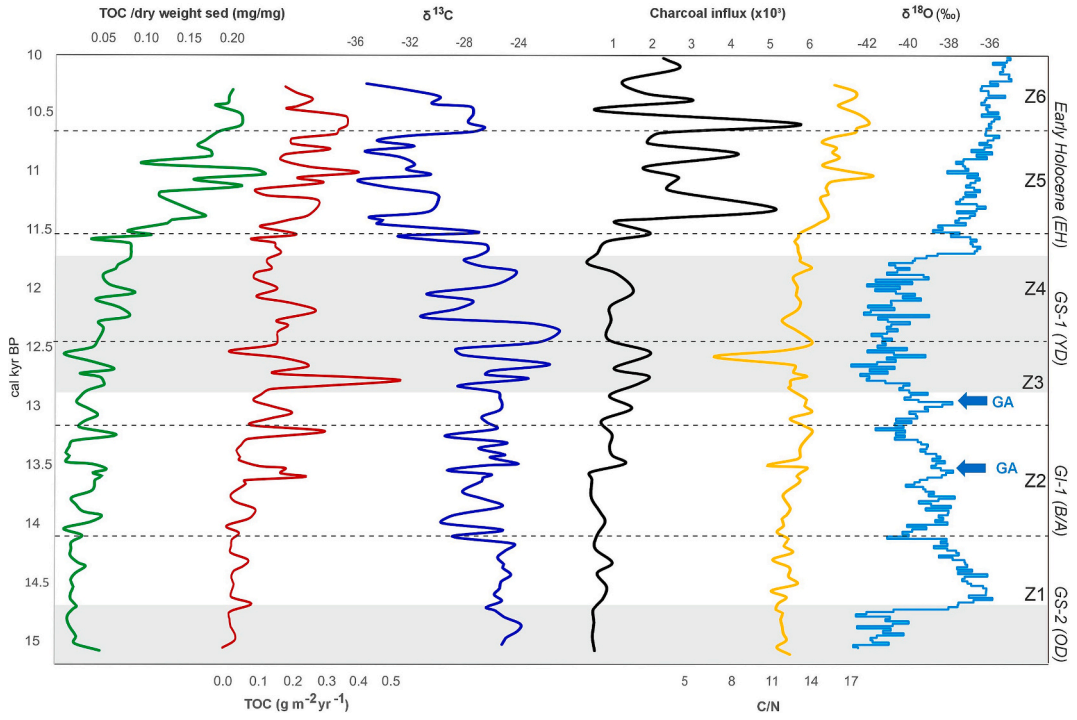

Fig. 4. TOC content (mg DW), TOC influx, C:N atomic ratio, $\delta^{13}C$ (‰), influx of charcoal particles, and climatic sequence of stadial-interstadial events that occurred between the Last Glacial Maximum (LGM) and the onset of the Holocene epoch (INTIMATE).

3.2. Diatoms

A total of 159 species were identified, with benthic species being clearly prevalent. A stratigraphic diagram of the most common diatom taxa observed (3 %) is provided (Fig. 6). Fluctuations in the relative abundances of diatom species and derived hydrological indicators enabled the distinction of four statistically differentiated zones (D1–D4) along the core (Bennett, 2002). The results are presented in chronological order.

3.2.1. Zone D1: six samples, 1100–1083 cm, c. 15.0–14.6 cal kyr BP

This zone is characterized by an abundance of Fragilariods and the lowest values of the centric/pennate ratio. *Staurosira brevistriata* (30–70 %) dominated the community, followed by *Staurosira robusta* (15 %), *Staurosira mutabilis* (10 %), *Staurosira lapponica* (7 %) and Staurosira venter (5 %). Other diatoms, such as *Sellaphora laevissima* (7 %) and *Achnanthes pusilla* (5 %), were found in minor proportions.

3.2.2. Zone D2: twenty-three samples, 1077–910 cm, c. 14.4–12.2 cal kyr BP

During this period, the centric/pennate ratio (10 %) increased from 1000 to 1070 mm, and the ratio of crysophytes to pennate diatoms reached 60 % by 950 mm. The Fragilarioid species shifted to *S. brevistriata*, *S. robusta* and *S. venter*. Other species notably increased, such as *Achnanthes minutissima* (20 %), *Achnanthes pusilla* (20 %), *Nitzschia palea* (30 %), *Nitzschia fonticola* (15 %), and *Discostella pseudostelligera* (10 %).

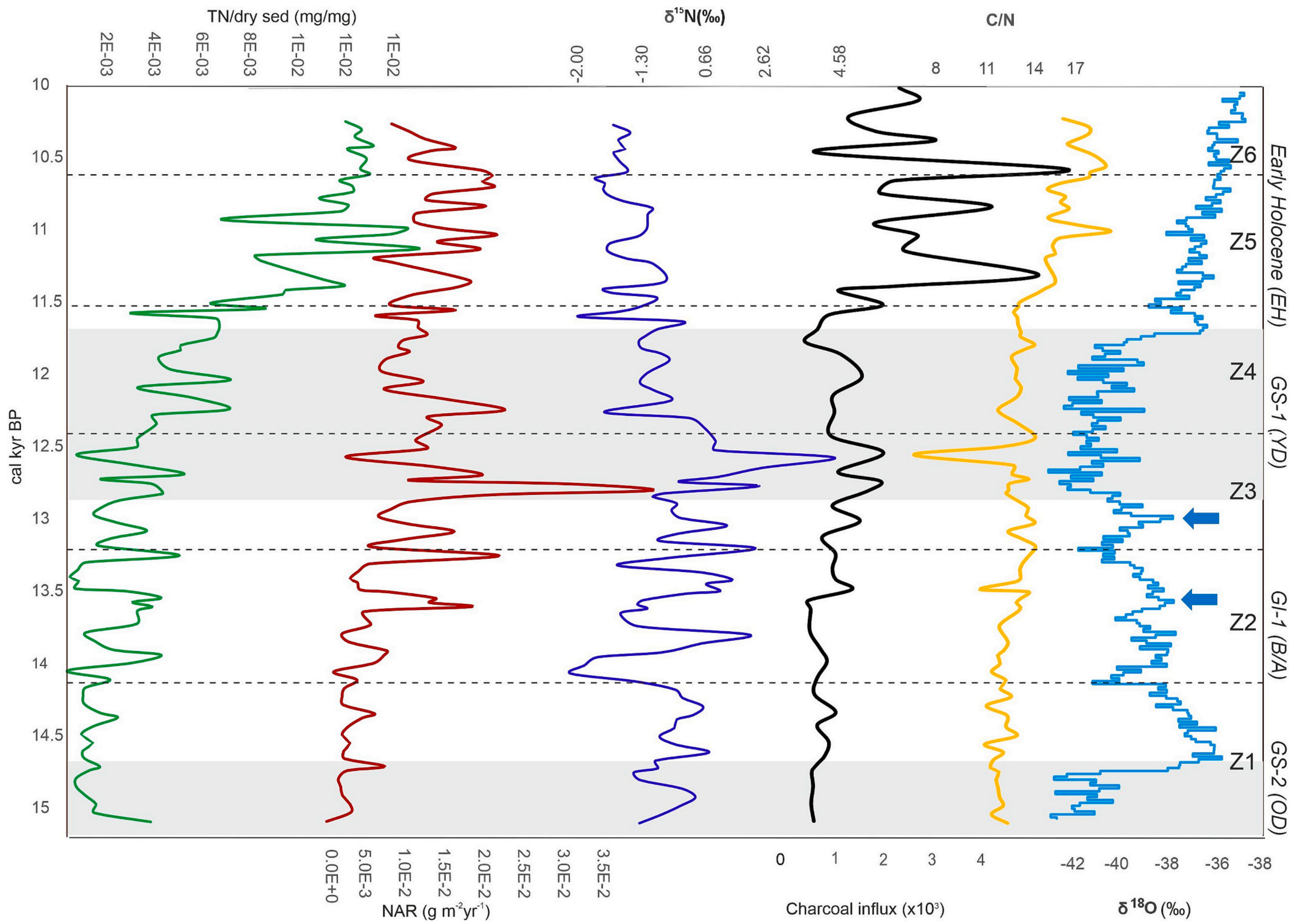

Fig. 5. TN content (mg DW), TN influx, C:N atomic ratio, $\delta^{15}N$ (‰), influx of charcoal particles, and climatic sequence of stadial-interstadial events that occurred between the Last Glacial Maximum (LGM) and the onset of the Holocene epoch (INTIMATE).

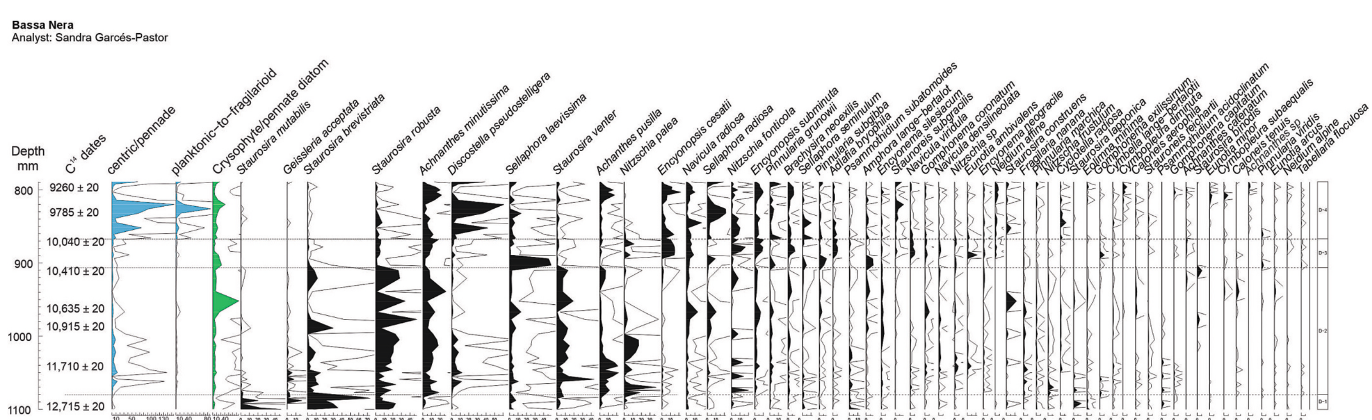

Fig. 6. Relative abundances (≥3 %) of diatom taxa throughout the Bassa Nera record. Solid lines are x100 exagerations.Dotted horizontal lines delimit four statistically significant zones (Bennett, 1996).

3.2.3. Zone D3: seven samples, 868–903 cm, c. 12.0–11.4 cal kyr BP

This brief period experienced decreases in both the centric/pennate and the crysophyte/pennate ratios. Fragilariod species decreased, and the community was dominated by *Sellaphora laevissima* (40 %), *Nitzschia palea* (10 %), *Encyonopsis cesatii* (15 %), *Navicula radiosa* (10 %), *Sellaphora radiosa* (10 %), *Nitzschia fonticola* (10 %), *Encyonopsis subminuta* (15 %), *Brachysira neoexilis* (7 %), *Pinnularia subgibba* (5 %), *Adlafia bryophila* (5 %) and *Amphora lange-bertalot* (5 %).

3.2.4. Zone D4: fifteen samples, 789–866 cm, c. 11.4–10.0 cal kyr BP

In this zone, there were sharp increases in the centric/pennate (150) and planktonic/fragilariod (80) ratios, whereas the cryophyte/pennate ratio (20 %) remained stable. The community was dominated by *Discostella pseudostelligera* (60 %), *Achnanthes minutissima* (20 %), and *Sellaphora laevissima* (10 %), with *Achanthes pusilla* (20 %) and *Encyonopsis cesatii* (15 %) increasing by the end of the zone. *Sellaphora radiosa* (20 %), *Nitzschia fonticola* (10 %) and *Encyonopsis subminuta* (7 %) were

also notable.

3.3. Principal component analysis

PCA helped identify relationships among biogeochemical and palynological indicators, dominant diatom taxa, and climate (Fig. 7). The first three principal components account for 70.2 % of the variance (PC1: 40.7 %, PC2: 20.0 %, PC3: 9.45 %). Shifts in TOC, TN, CAR, NAR, and C/N ratios are mainly captured by the first component (C1), with increasing importance towards its positive side. Forest groups F1 and F2 and charcoal correlate with the positive end of C1, while $\delta^{13}C$ and $\delta^{15}N$ show opposite relationships. Fragillarioid diatoms plot towards the negative side of C1, whereas centric diatoms and the C/P ratio align with the positive side. The second component (C2) separates algae and open vegetation types (O1 and O2) from forest taxa. Sample scores follow a chronological sequence along C1, with older samples on the left and younger ones on the right. Ecologically, C1 reflects a transition from low-productivity, open environments towards wetter, more productive conditions that favoured forest expansion and lake development in the Early Holocene, while C2 distinguishes open Younger Dryas landscapes from closed forested environments.

4. Discussion

4.1. Biogeochemical indicators and climatic changes

Based on these results, we discuss how the different INTIMATE climatic events and glaciation cycles could have affected the biogeochemical indicators, carbon–nitrogen dynamics and organic matter development. All $\delta^{13}C$ values (−20 to −36 ‰) remain within the C_3 range, excluding any C_4 contribution (Kohn, 2010; Diefendorf et al., 2010).

4.1.1. Stadial GS-2 (Oldest Dryas); c. 17.5– to 14.7 cal kyr BP

The beginning of our record (Z1) is coeval with the cold Heinrich event 1 (H1) at approximately 15.0 cal kyr BP. H1 occurred around 16 to approximately 16–13 kyr ago and was marked by massive discharges of icebergs from the Laurentide Ice Sheet into the North Atlantic. The influx of fresh water from melting icebergs weakened the Atlantic Meridional Overturning Circulation, leading to significant cooling in the Northern Hemisphere. H1 had widespread climatic impacts, contributing to abrupt temperature changes and altering precipitation patterns (Bond et al., 1993; Hemming, 2004). This climatic perturbation impacted the Mediterranean thermohaline circulation (Sierro et al., 2005) and the Pyrenees, as shown by the OST2 record (Fig. 2) (Bernal-Wormull et al., 2021). By 14.5 ± 06 kyr, deglaciation in the eastern Pyrenees was nearly finished by GI-1; only minor glaciers remained until approximately 12.3 kyr ago in cirques where specific local conditions supported their persistence (Reixach et al., 2021).

During the initial deglaciation, the Pla dera Muntanheta area experienced persistent harsh and cold climates, as well as glacial retreat. Sedimentation began on bare rock in a proglacial pond formed in front of retreating moraines. The sediment material was lithostratigraphic described as clastic, with no apparent organic matter and only scant pollen concentrations (Rull et al., 2023). Further evidence supporting the geogenic origin of the BN peat bog (in depressions and receiving water that had been in contact with mineral bedrock or soils) (Joosten and Clarke, 2002) is the slowness, on the order of millennia, in the formation of a substrate susceptible to colonization by locally rooted vegetation. The observed amounts of TOC, TN, CAR and NAR were extremely low. In fact, diverse palynological data from the same sediment and depth (Rull et al., 2023) suggest that organic matter supplies came from scattered, periglacial, grassy *Artemisia* stands, and from fungal spores and algae (*Pediastrum, Zygnema, Botryococcus*) thriving in one or several small oligotrophic puddles. At that time, arboreal pollen had not yet reached high mountain areas; the pine forest treeline was estimated to be 1500 m lower than it is today, and deciduous forests were probably farther away. Regional charcoal particles were also very scarce. The low values of centric-to-pennate and crysophyte-to-pennate diatom ratios suggest low water levels. This agrees with the presence of epilithic and opportunistic small Fragilarioids (*Staurosira brevistriata, S. robusta, S. mutabilis, S. lapponica,* and *S. venter*), with some *S. laevissima and A. pusilla* associated with alkaliphilous and fresh brackish water bodies (Van Dam et al., 1994).

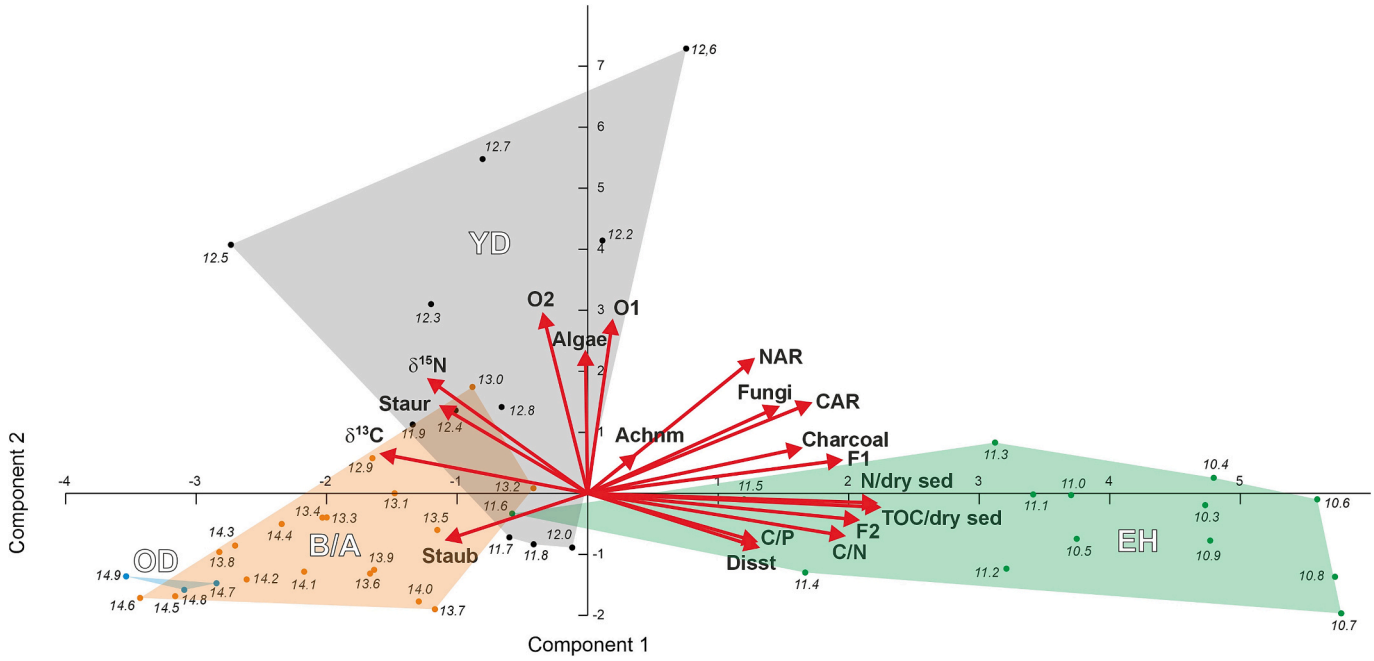

Fig. 7. Principal Component Analysis on bioeochemical variables, environmental indicators, and diatom species. The colored polygons indicate a progression in the age of the samples along axis C1 from left to right, clearly organizing them according to the climatic periods they represent. Blue: OD (GS-2), pink: B/A (GI-1), purple: YD (GS-1), green: EH. (For interpretation of the references to colour in this figure legend, the reader is referred to the web version of this article.)

4.1.2. Interstadial GI-1 (B/A); c.14.7– to 12.9 cal kyr BP

The first abrupt warming of the LG had a minimal impact on the biogeochemical indicators (Z1). At the B/A onset, approximately 14.7 cal kyr BP in the western Pyrenees (Bernal-Wormull et al., 2021) (Fig. 2), temperatures sharply rose across the North Atlantic, Europe and Greenland, coinciding with moisture deficits in central and southern Europe (Naughton et al., 2009, 2016, 2023). Accordingly, the mean $\delta^{18}O$ speleo amplitude at Osolo cave (western Pyrenees) was 2.43 ‰ and ranged from −6.67 ‰ to −4.23 ‰, suggesting a temperature change of approximately 7.5 °C over 50 years (Bernal-Wormull et al., 2021). At BN, biogeochemical data indicate that the organic substrate was quite thin, which substantially limited plant growth and diversification despite the significant increase in temperature. However, this situation changed when the TOC and TN contents and accumulations began increasing and fluctuating (Z2), likely because of landscape shifts resulting from forest refugia that ascended to the mountains, mainly pine forest. In fact, rooting into the substrate began during the B/A interstadial (Rull et al., 2023). The marked shifts in the targeted variables along Z2 were consistent with the pronounced climatic instability of the B/A, as observed when the data were compared with the NGRIP2 and OST2 records (Fig. 1). For example, at approximately 13.5 cal kyr BP, noticeable decreases in TOC, TN, CAR, NAR, and C/N, along with increases in carbon and nitrogen isotopic values, suggest more open vegetation a reduction in organic matter inputs, and unfavourable environmental conditions for soil formation. Additionally, a slight increase in charcoal particles indicates an increase in regional fires. All these changes coincided with local glacier advance. Notably, some glaciers advanced and still interrupted the deglaciation trend that began after the LGM at approximately 13.5 and 13.0 cal kyr BP (GI-1.c1 and GI-1. a, respectively) (Fig. 1). The existence of these cooling episodes at BN was evidenced by moraine systems situated in the adjacent Ruda Valley at elevations of 2080 m and 2190 m (Fernandes et al., 2022). Consequently, the glacier fronts would have been positioned 190 m and 300 m higher than the Bassa Nera peat bog, respectively (Rull et al., 2023). The cooling linked to the first advance/retreat of the glacial episode lasted for a couple of centuries, and the second advance/retreat occurred during the climatic transition towards the Younger Dryas (YD). The increases in centric-to-pennate and crysophyte-to-pennate diatom ratios, as well as the presence of planktonic *D. pseudostelligera,* indicate an increase in the water column. The changes in the diatom community suggest a shift towards circumneutral fresh water.

4.1.3. Stadial GS-1 (YD); c. 12.9–11.7 cal kyr BP

Regionally, the Younger Dryas stadial was characterized by cooler temperatures, an increased humidity trend and significant climatic shifts (Fig. 1). Interestingly, our biogeochemical indicators displayed two clearly differentiated patterns of variation along zones Z3 and Z4. At the onset of storage, the TOC and TN contents did not change significantly. In contrast, pronounced shifts in the C/N ratios, isotopic values and CAR and NAR values were detected. The lower C/N ratios suggest qualitative changes in the sources of organic matter inputs, with the conspicuous minimum coinciding with a notable growth of chrysophytes and with higher values of $\delta^{13}C$ and $\delta^{15}N$. While planktonic diatoms may have contributed to this signal, our record indicates that they alone cannot explain the pronounced C/N minimum. The simultaneous expansion of chrysophytes (Fig. 6) and other non-diatom algae (Fig. 2) evidenced in the palynological record likely exerted a stronger influence on organic matter quality. At the same time, the modest increase in TOC and TN contents, contrasted with higher fluxes, suggests that the dominant inputs consisted of labile organic matter readily decomposed in the sediment, such as algal cells or tissues poor in cellulose and lignin. These results are consistent with a shift towards more humid conditions documented in the Sesolo Cave record and align with the palynological evidence, which shows concurrent accumulations of algae and sediments, increased local runoff and moisture, and a notable expansion of open vegetation dominated by *Artemisia* and Poaceae (O1) (Fig. 3). This milder and moister episode ended abruptly by 12.6 cal kyr BP and gave way to the coldest spell of the YD in the Pyrenees (Fig. 1). Neighbouring pine forests shrank and/or descended to lower altitudes, permafrost conditions expanded, and the water level at the BN pond diminished. All these changes possibly altered the sources, processing and isotopic fractionation of C and N in the sediment. Indeed, decreases in almost all biogeochemical indicators occurred, except for a marked positive excursion of $\delta^{15}N$. An increase in the $\delta^{15}N$ values to 4.58 ‰ may indicate isotopic fractionation during remineralization of organic nitrogen, e.g., due to organisms' preference for ^{14}N or changes in isotopic equilibrium among different inorganic forms of nitrogen. In anaerobic environments, denitrification also enriches gaseous nitrogen in ^{15}N because microorganisms favour ^{14}N as an energy source (Hu et al., 2020). In fact, anaerobic conditions have been reported for the 12.9– to 12.4 kyr BP interval (Vegas-Vilarrúbia et al., 2024). Interestingly, Chenopodiaceae were prominent in the O2 palynological assemblage (Fig. 3), and nitrophilous species were included among the species in this family (Rull et al., 2023). After 12.5 kyr BP, a gradual warming trend arose that marked the termination of the GS-1 stadial. The values of TOC and TN and their respective accumulation rates concurred with the amelioration of living conditions, with slow increases and slight fluctuations. Two positive $\delta^{13}C$ peaks coincided with new algal growth and other aquatic vegetation by 12.3 and 11.9 cal kyr BP, indicating new episodes of enhanced local runoff and moisture (Rull et al., 2023). The $\delta^{15}N$ values returned to approximately 0 ‰, suggesting cessation of denitrification, minimal microbial activity and/or direct cyanobacterial N fixation (Craine et al., 2015). In summary, during the GS-1 period (YD), the biogeochemical indicators exhibited highly variable and distinctive fluctuation patterns, which were significantly influenced by the sources and processing of carbon and nitrogen in the Bassa Nera pond. These variations were associated with the emergence of short, wet climate episodes amid an overall cold and dry climate followed by an increasing precipitation trend (Fig. 2). These variations had considerable impacts on vegetation assemblages (Rull et al., 2023). The YD featured a sudden rise in temperature that was not parallel to the comparable increases in the biogeochemical variables. The decrease in the centric-to-pennate diatom ratio and the increases in epilithic species such as *S. laevissima, E. cesatii, N. fonticola* and *E. subminuta* suggest a decrease in the water level while maintaining circumneutral conditions.

4.1.4. Early Holocene (EH) (11.7– to 10.2 cal kyr BP)

The rather smooth changes in biogeochemical variables during the initial decades of the Early Holocene (EH) were abruptly interrupted by a general decrease in values between 11.5 and 11.4 kyr BP (Z5). Following these negative shifts, there was a rapid increase and sharp oscillation trend, with peaks occurring between 11.2 and 11 kyr BP in total organic carbon (TOC), total nitrogen (TN), their accumulation rates, and $\delta^{13}C$ values. Interestingly, some of these abrupt changes seem to be related to features of the preboreal oscillation (PBO), a brief but notable cooling anomaly impacting the North Atlantic region immediately after the end of GS-1 (Rasmussen et al., 2007). The PBO also affected the Iberian Peninsula, as evidenced by conspicuous changes in vegetation and hydrology (López-Sáez et al., 2020). This event was characterized by a temporary return to low $\delta^{18}O$ values between 11.5 and 11.4 kyr BP and ended with a short period of very high $\delta^{18}O$ values at approximately 11.2 kyr BP. The most significant impact of the PBO was likely rapid shifts in the composition of organic matter sources, as evidenced by a small retreat of the still-reduced deciduous forest in favour of the pine forest and a reduction in the O1 assemblage (Fig. 3).

Subsequent climatic oscillations (Z5 and Z6) likely affected the biogeochemical indicators until the end of the record. The TOC and TN contents and accumulation increased in accordance with the warming trends. The $\delta^{13}C$ and $\delta^{15}N$ values shifted moderately towards more negative values. The most negative $\delta^{13}C$ values (< -30 ‰) in the Early Holocene coincided with the expansion of conifer and deciduous taxa (Rull et al., 2023), indicating that these $\delta^{13}C$ values reflect significant

shifts in C_3 forest composition, rather than changes between C_3 and C_4 plant types.

The expansion of deciduous forests, along with the first significant increase in fire incidence (Fig. 3; Rull et al., 2023), reflects broader ecosystem changes that introduced new carbon and nitrogen sources at the onset of the Holocene. However, since most charcoal particles were < 150 μm, these fires are likely indicative of regional burning of deciduous forests, with minimal evidence of local fire activity. The 191 % increase in carbon accumulation is therefore best attributed to enhanced productivity and organic matter input under warmer conditions and forest expansion. In this context, fire likely acted as a regional background process, contributing little to nutrient release within the mire.

The significant increases in the centric-to-pennate, planktonic-to-fragilarioid and crysophyte-to-pennate diatom ratios, along with the presence of *D. pseudostelligera*, indicate a notable rise in the water level not observed in the previous zones. It has been hypothesized that the greater abundance of *D. pseudostelligera* was associated with greater nitrogen availability, possibly associated with in-lake N fixation by cyanobacteria (e.g., *Nostoc* species) and terrestrial N fixers, such as *Dryas* species (Fritz and Anderson, 2013).

4.2. Significance of carbon storage in the pre-peat environment of the Bassa Nera peat bog

The Bassa Nera (BN) site provides crucial insights into carbon storage dynamics in pre-peat environments. Understanding these dynamics is essential for reconstructing past climates, studying ecosystem responses to climatic shifts, and modelling future carbon cycling and storage. Overall, the shift in atmospheric CO_2 from the LGM to the Holocene is well established in both hemispheres. The high-resolution record in the ice core EPICA Dome Concordia (Dome C) shows how the CO_2 levels climbed from 189 ppmv to 265 ppmv between 18.1 and 11 kyr BP and then stabilized at 280 ppm over the Holocene until the preindustrial period. This increase occurred in four steps (Monnin et al., 2001). From 17 to 15.4 kyr BP, CO_2 rose from 189 to 219 ppmv at 20 ppmv/kyr.

Our organic carbon record at BN started later, by 15 kyr BP, and was concurrent with the second increase in atmospheric CO_2 that took place between 15.4 and 13.8 kyr BP, with CO_2 increasing from 219 to 231 ppmv at a rate of 8 ppm/kyr. During that time, periglacial conditions prevailed in the high Pyrenean mountains (Fernandes et al., 2022). At BN, the bare rock ecosystem had a negligible capacity to act as a carbon sink or source, as evidenced by the low TOC concentration and accumulation values. Nor were there remnants of vegetation or organic matter from the preceding Eemian interglacial period that could represent an "occult" carbon reservoir. It has been hypothesized that during glaciations, advancing continental ice sheets buried organic carbon from vegetation and soils that were produced during preceding interglacials. These millennial carbon stocks would have then released CO_2 back into the atmosphere during the following interglacial period (Treat et al., 2019; Zeng, 2003, 2005, 2006). This was not the case for the BN peat bog. Like most geomorphological features of the Central-Eastern Pyrenees (Ventura and Turu, 2022), this basin was shaped by glacial action during the last MIS 2 stadial; thus, any organic material remaining from the former interglacial cycle was likely eroded, transported, and deposited downhill, leaving only bare rock on site. Therefore, it can be inferred that during GS-2, carbon exchange between the atmosphere and the incipient organic substrate of the BN peat bog was insignificant.

Noticeable increases in TOC content started at approximately 14 BP kyr in the middle of GI-1, as soon as conditions were favourable enough, i.e., water availability owing to glacial melting and temperature. From GS-2 to GI-1, the average TOC content and CAR values percentual increase were 30.2 % and 64.3 %, respectively, reflecting the impact of water availability and increased solar radiation on organic matter production, which ultimately favoured carbon storage, despite the climatic instability of this period showing a number of short-lived climatic oscillations (Rasmussen Clausen et al., 2014). Our results suggest that temperature oscillations and the remaining glacial activity led to a variety of feedback mechanisms of carbon gains and losses that resulted in a net increase in carbon in the sediment. For example, during colder sub-events of GI-1, like GI-1-d and b, aeolian deposition (e.g., mineral dust) and glacier readvances, as well as permafrost conditions (e.g., waterlogged, anaerobic soils), may have favoured organic carbon accumulation via the physical and chemical protection of organic matter from decomposition. Paradoxically, these conditions also restricted organic growth (Treat et al., 2019). In contrast, during warmer sub-events such as GI -2e, c3, and c1a, freeze–thaw cycles likely enhanced the mechanical breakdown and thermal decomposition of previously stabilized organic matter due to freezing temperatures. Additionally, hydrological changes such as meltwater production and the expansion and contraction of surrounding wetlands may have facilitated carbon leaching in the form of dissolved and particulate organic carbon (Davidson and Janssens, 2006; Zollinger et al., 2013). These mechanisms suggest a dynamic interplay between temperature fluctuations and hydrological changes, leading to alternating phases of carbon sequestration and release. Hypothetically, these mechanisms became significant between 15 and 13.8 kyr BP, facilitating exchanges of CO_2 between the atmosphere and sediment and paving the way for peatland inception.

The third phase involves the transition from GI-2 to GSI. Between 13.8 and 12 kyr BP, atmospheric CO_2 levels decreased slightly from 239 to 237 ppmv, but between 12.3 and 11.2 kyr BP, they significantly increased to 259 ppm at a rate of 20 ppmv per year. Concurrently, a 50 % percentual increase in sedimentary TOC content occurred despite an 8 % percentual decrease in CAR, that is, carbon influx to the sediment. The marked oscillation of CAR values suggests a certain ease of reversing the sense of carbon influxes and processes during this period (losses and gains of carbon), pointing to potential feedback effects with atmospheric CO_2. In fact, higher atmospheric CO_2 availability may have fostered primary production. Another likely explanation for this apparent discrepancy may be the deceleration in the breakdown of organic carbon molecules that had accumulated during earlier, warmer phases, leading to increases in the carbon stock. This may have been caused by factors such as temperature decrease, freezing and anaerobic conditions (Davidson and Janssens, 2006) during the cold GS-1 event. Interestingly, it was at the beginning of this stage when the system briefly became the largest sink for TOC during the entire period of study.

At this developmental stage and amidst rising atmospheric CO_2 levels, a pivotal feature of peat formation emerged at BN: dead plant matter accumulated at a faster rate than it decomposed. This trend became even more evident from the second half of GS-1 to the EH interglacial stage, with a notable 191 % percentual increase in the average TOC concentration and a new decrease of 14 % in the CAR average value. It is beyond the scope of this study to discuss whether, at that time, the BN wetland was already a "true peatland," given that criteria for defining a peatland today are still highly debated (Lourenco et al., 2023). However, it is worth mentioning that this was the first time that the carbon content in BN sediments met the FAO (1998) criteria for organic soils (12–18 %) based solely on organic carbon; this occured approximately 11.4 kyr BP. This result strongly indicates that the BN peatland system began sequestering carbon before 10 kyr BP, during the cold PBO anomaly. Until 10.2 kyr BP (i.e., the end of the record), the percentage of organic carbon in the soil subsequently increased to an average of 17.6 %, reaching a maximum of 23.9 %.

4.3. Comparison with other peatlands of Southern Europe

Among southern European countries, the presence of peatlands varies and is rare. Spain, Portugal, Italy and France together have an estimated 6051 km^2 of peat and peat-topped soils with >20 % organic carbon (histosols), which is relatively low compared with Scandinavia's 85.635 km^2 or Finland's 88.098 km^2 (Montanarella et al., 2004). Consequently, southern European peatlands are often overlooked in data collection and research efforts; thus, their actual coverage may be

underestimated (Chico et al., 2020). In addition, the scarcity of studies and data on peatlands in southern Europe hampers the possibility of making robust and insightful comparisons concerning peat accumulation, formation and dynamics over time. Most existing research has concentrated on Holocene peatlands in northern regions, with recent attention increasingly shifting towards tropical peatlands (e.g., Loisel et al., 2017; Morris et al., 2018; Treat et al., 2019). This emphasis further exacerbates the challenge of understanding peatlands in southern Europe. Against this backdrop, our BN record spans only ~1500 years of the Early Holocene and reflects a minerogenic setting; therefore, the accumulation rates we report (~0.2 g C m^{-2} yr^{-1}) are not directly comparable to those from northern peatlands. For instance, Loisel et al. (2014) present Holocene-long means of 23 ± 2 g C m^{-2} yr^{-1} with Early Holocene peaks of 25–28 g C m^{-2} yr^{-1}, while Longman et al. (2021) document values exceeding 120 g C m^{-2} yr^{-1} in central–eastern European mountain peatlands. These estimates should thus be regarded as contextual reference, highlighting the distinctive depositional environments of southern mountain peatlands. Considering that Bassa Nera is an alpine peat bog located at 1890 m a.s.l., it is reasonable to assume that the mechanisms of peat initiation may be similar to those of boreal peatlands owing to their similar climatic conditions. Most peatland onset in northern Europe (NE) occurred following the retreat of the Scandinavian ice sheet at approximately 18 kyr BP and experienced rapid establishment in the first half of the Holocene (Ruppel et al., 2013; Treat et al., 2019). Our stratigraphic record at BN extends back only 15 kyr but exhibits comparable trends and has no gaps (Vegas-Vilarrúbia et al., 2024). With respect to its origin, three processes have been proposed for peat formation in northern Europe (NE) and North America (NA): i) primary mire formation, which is tied to physical processes such as ice sheet retreat; ii) terrestrialization, which results from long-term water body infilling; and iii) paludification or expansion of bogs due to rising water tables (Ruppel et al., 2013). Given that the sediments at the bottom of our PATAM12-A-14 core were in direct contact with granitic bedrock and were described as clastic without organic matter (Rull et al., 2023), the initiation of the BN peat bog aligns well with the primary mire formation mechanism. Pontevedra-Pombal et al. (2017) applied these same processes to explain the genesis, evolution and types of 108 representative Iberian peatlands, among which 45 % belong to the Atlantic biogeographical region and 8 % to the Alpine biogeographical region. The timing of their formation varied: bogs appeared only in the early and late Holocene, whereas fens formed from the Late Glacial period (very few) to the Little Ice Age.

For comparison, in this work, we examined peat bog core site information with Late Glacial pollen data from the Eurosiberian biogeographic region, in the Pyrenees above 1000 m a.s.l., as reported by Rull et al. (2023) (Fig. 1).

We searched for data on organic carbon content, accumulation rates and peat onset estimations to determine approximately when, if available, organic carbon compatible with the presence of peat occurred. In most cases, these data were unavailable, the published records had low resolution, or only lithostratigraphic descriptions of organic-rich or peat sediments were provided. For example, the Portalet peat bog in the central-western Spanish Pyrenees contained lake sediment with organic matter exceeding 20 %. This organic content increased after 13.5 kyr BP and transitioned into peat by approximately 6.5 cal. kyr BP (González-Sampériz et al., 2006). In Navamuño peat bogs in the Iberian Central System, organic clays appeared c. 15.7 cal kyr BP and evolved into dark brown, organic matter-rich sediments in a marshy environment at approximately 14.9 cal kyr BP (Turu et al., 2018). Beyond the Iberian Peninsula, in the biogeographic alpine region (>1500 m a.s.l.) of the Mediterranean Alps, a study of sixteen lacustrine and mire sediment records spanning the LG-H period revealed that soil formation had begun in the PBO from 13 to 8.7 cal kyr BP. The influence of the kyr BP glacial period on lake sediments declined and increasing biogenic processes and organic-rich sediment deposition started later, at approximately 11.5 cal kyr BP. Additionally, the altitudinal gradient and catchment exposure (north- or south-facing) significantly influenced the timing of organic-rich lithotype onset, with a delay of ±2000 years (Brisset et al., 2015). Another survey in the eastern French Pyrenees and the Massif Central reported sediments rich in organic detritus associated with the LG period, yet no peatland as such was documented (Reille and Lowe, 1993). Similarly, a peat bog multiproxy record from Danta peat bogs in the northeastern Italian Alps (Dolomites, >1400 m a.s.l.) indicates that gyttja accumulation began between ca. 13.2 and 10.6 kyr BP, with a transition to decomposed peat occurring between 9.7 and 9.5 kyr BP (Poto et al., 2013). Hence, in general terms, these findings broadly align with the onset of organic sediment in the BN peat bog, where the organic carbon content exceeded 12–18 % at approximately 11.4 kyr BP. However, from our literature review, although limited, it seems evident that total carbon or organic carbon data documenting pre-Holocene carbon dynamics in mountain peat areas of southern Europe are very scarce, which does not mean that they cannot be obtained. In line with this, mountainous peatlands are significantly less studied than lowland peatlands because of their remote locations and topography, and only a few studies have explored their carbon dynamics (Chimner et al., 2010).

Finally, the BN peat bog is among the deepests one in Europe, being the average depth 3-4 m. The deepest peatland in Europe is Philippi peatland (Greece) with 234 km^2 and up to 190 m. Peatlands with a small surface area but above-average peat thickness potentially have a greater carbon storage capacity than expected based solely on their area. These peatlands may be more common than previously thought and could represent a unique opportunity to enhance our understanding of long-term carbon dynamics. For example, the Philippi peatland showcased the transition from peat to coal (Melidonis 1981, in UN, 2022). This case highlights that peat depth is an important variable to consider from now on.

5. Conclusions

We tracked TOC and TN dynamics over 5000 years (LG–EH) from a continuous record at the Bassa Nera peat bog. This undisturbed sequence reveals clear links between organic matter accumulation and climatic–ecological shifts.

C/N and $\delta^{13}C$ values indicate mixed terrestrial and aquatic inputs in early peat development, while low $\delta^{15}N$ suggests limited metabolic activity. Extremely low carbon accumulation rates point to external sources dominating the first organic layers.

At the onset of the Holocene, carbon accumulation rose sharply, consistent with other Northern Hemisphere sites. Yet nearly five millennia of physical and biochemical processes—largely independent of human impact—were required before the system could retain enough carbon to sustain peat growth.

Organic carbon dynamics were non-linear, responding directly to climate: cold, unstable phases depressed accumulation and activity, whereas warming and stabilization enhanced carbon storage. BN development began earlier than most peatlands, with milestones at ~14 kyr BP (first organic layers), 12.3–11.2 kyr BP (TOC accumulation outpacing decomposition), and intensified sequestration during late GS-1 to EH, leading to true peat initiation before 10 ka BP.

Peatlands with small surface areas but substantial thickness may store more carbon than expected, highlighting the importance of depth-based mapping. This has implications for refining global carbon storage estimates. Finally, peat accumulation is an extremely slow process: restoration of degraded peatlands may take centuries, and full recovery of carbon storage capacity should not be expected in the short term.

CRediT authorship contribution statement

Teresa Vegas-Vilarrúbia: Writing – review & editing, Writing – original draft, Supervision, Project administration, Methodology, Investigation, Funding acquisition, Formal analysis, Conceptualization.

Arnau Blasco: Methodology, Investigation, Formal analysis. **Sandra Garcés-Pastor:** Writing – review & editing, Writing – original draft, Methodology, Investigation, Formal analysis. **Maarten Blaauw:** Writing – review & editing, Methodology, Investigation, Formal analysis. **Miguel Ángel Calero:** Writing – review & editing, Methodology, Investigation, Formal analysis. **Valentí Rull:** Writing – review & editing, Methodology, Investigation, Funding acquisition, Formal analysis, Conceptualization.

Funding

Autonomous Organization of National Parks (OAPN), project LACEN (OAPN-2450S); Institute of Catalan Studies (IEC), project POLMONT-2012; Management of University and Research Grants Agency (AGAUR), projects GREB-2014 SGR 514 and GREB-2021 SGR 00315.

Declaration of competing interest

The authors have nothing to declare.

Acknowledgements

We thank fieldwork and laboratory collaborators, Núria Cañellas-Boltà, Encarni Montoya, Nick Loughlin, Arantza Lara and Julià López-Vila. SGP was supported by the Beatriu de Pinós Programme (BP-2021-00131). We thank the referees for their valuable comments.

Appendix A. Supplementary data

Supplementary data to this article can be found online at https://doi.org/10.1016/j.palaeo.2025.113330.

Data availability

Raw data are available upon request to T.V-V.

References

Bartolomé, M., Moreno, A., Sancho, C., Stoll, H.M., Cacho, I., Spötl, C., Belmonte, Á., Edwards, R.L., Cheng, H., Hellstrom, J.C., 2015. Hydrological change in Southern Europe responding to increasing North Atlantic overturning during Greenland Stadial 1. Proc. Natl. Acad. Sci. USA 112, 6568–6572. https://doi.org/10.1073/pnas.1503990112.

Bennett, K.D., 1996. Determination of the number of zones in a biostratigraphical sequence. New Phytol. 132, 155–170.

Bennett, K.D., 2002. Documentation for Psimpoll 4.10 and Pscomb1.03. C Programs for Plotting Pollen Diagrams and Analysing Pollen Data. University of Cambridge, Cambridge.

Bernal-Wormull, J.L., Moreno, A., Pérez-Mejías, C., Bartolomé, M., Aranburu, A., Arriolabengoa, M., Iriarte, E., Cacho, I., Spötl, C., Edwards, R.L., Cheng, H., 2021. Immediate temperature response in northern Iberia to last deglacial changes in the North Atlantic. Geology 49, 999–1003. https://doi.org/10.1130/G48660.1.

Blaauw, M., Christen, J.A., 2011. Flexible paleoclimate age-depth models using an autoregressive gamma process. Bayesian Anal. 6, 457–474.

Blodau, C., 2002. Carbon cycling in peatlands — a review of processes and Controls. Environ. Rev. 10, 111–134. https://doi.org/10.1139/A02-004.

Bond, G., Broecker, W., Johnsen, S., McManus, J., Labeyrie, L., Jouzel, J., Bonani, G., 1993. Correlations between climate records from North Atlantic sediments and Greenland ice. Nature 365, 143–147. https://doi.org/10.1038/365143a0.

Brisset, E., Guiter, F., Miramont, C., Revel, M., Anthony, E.J., Delhon, C., Arnaud, F., Malet, E., De Beaulieu, J.L., 2015. Lateglacial/Holocene environmental changes in the Mediterranean Alps inferred from lacustrine sediments. Quat. Sci. Rev. 110, 49–71. https://doi.org/10.1016/j.quascirev.2014.12.004.

Carrillo, E., Carreras, J., Ferré, A., Ninot, J.M., Pérez Haase, A., 2008. Singularitat de la vegetació de les reserves integrals de Trescuro i d'Aiguamòg. In: Jornades sobre recerca al Parc Nacional d'Aigüestortes i Estany de Sant Maurici. 25–27 October. Vall de Boí, Barruera, pp. 177–192.

Carrión, J.S., Fernández, S., González-Sampériz, P., Gil-Romera, G., Badal, E., Carrión-Marco, Y., López-Merino, L., López-Sáez, J.A., Fierro, E., Burjachs, F., 2020. Expected trends and surprises in the Lateglacial and Holocene vegetation history of the iberian Peninsula and Balearic Islands. Rev. Palaeobot. Palynol. 162, 458–475. https://doi.org/10.1016/j.revpalbo.2009.12.007.

Chico, G., Clutterbuck, B., Clough, J., Lindsay, R., Midgley, N.G., Labadz, J.C., 2020. Geo-hydromorphological assessment of Europe's southernmost blanket bogs. Earth Surf. Process. Landf. 45, 2747–2760. https://doi.org/10.1002/esp.4927.

Chimner, R.A., Lemly, J.M., Cooper, D.J., 2010. Mountain fen distribution, types and restoration priorities, San Juan Mountains, Colorado, USA. Wetlands 30, 763–771. https://doi.org/10.1007/s13157-010-0039-5.

Clymo, R.S., Turunen, J., Tolonen, K., 1998. Carbon accumulation in peatland. Oikos 2, 368–388.

Craine, J.M., Brookshire, E.N.J., Cramer, M.D., Hasselquist, N.J., Koba, K., Marin-Spiotta, E., Wang, L., 2015. Ecological interpretations of nitrogen isotope ratios of terrestrial plants and soils. Plant Soil 396, 1–26.

Davidson, E.A., Janssens, I.A., 2006. Temperature sensitivity of soil carbon decomposition and feedbacks to climate change. Nature 440, 165–173. https://doi.org/10.1038/nature04514.

Diefendorf, A.F., Mueller, K.E., Wing, S.L., Koch, P.L., Freeman, K.H., 2010. Global patterns in leaf ^{13}C discrimination and implications for studies of past and future climate. Proc. Natl. Acad. Sci. 107, 5738–5743. https://doi.org/10.1073/pnas.0910513107.

FAO, 1998. World Reference base for Soil Resources. World Soil Resources Reports No. 84. Food and Agriculture Organization of the United Nations, Rome.

Fernandes, M., Oliva, M., Vieira, G., Palacios, D., Fernández-Hernández, J.M., Garcia-Oteyza, J., Schimmelpfennig, I., Team, A., Antoniades, D., 2022. Glacial oscillations during the Bølling-Allerød Interstadial-Younger Dryas transition in the Ruda Valley, Central Pyrenees. J. Quat. Sci. 37, 42–58.

Fritz, S.C., Anderson, N.J., 2013. The relative influences of climate and catchment processes on Holocene lake development in glaciated regions. J. Paleolimnol. 49, 349–362.

Garcés-Pastor, S., Cañellas-Boltà, N., Pèlachs, A., Soriano, J.M., Pérez-Obiol, R., Pérez-Haase, A., Calero, M.A., Andreu, O., Escolà, N., Vegas-Vilarrúbia, T., 2017. Environmental history and vegetation dynamics in response to climate variations and human pressure during the Holocene in Bassa Nera, Central Pyrenees. Palaeogeogr. Palaeoclimatol. Palaeoecol. 479, 48–60. https://doi.org/10.1016/j.palaeo.2017.04.016.

González-Sampériz, P., Valero-Garcés, B.L., Moreno, A., Jalut, G., García-Ruiz, J.M., Martí-Bono, C., Delgado-Huertas, A., Navas, A., Otto, T., Dedoubat, J.J., 2006. Climate variability in the Spanish Pyrenees during the last 30,000 yr revealed by the El Portalet sequence. Quat. Res. 66, 38–52. https://doi.org/10.1016/j.yqres.2006.02.004.

Gorham, E., 1991. Northern peatlands: role in the carbon cycle and probable responses to climatic warming. Ecol. Appl. 1, 182–195. https://doi.org/10.2307/1941811.

Gorham, E., Lehman, C., Dyke, A., Janssens, J., Dyke, L., 2007. Temporal and spatial aspects of peatland initiation following deglaciation in North America. Quat. Sci. Rev. 26, 300–311. https://doi.org/10.1016/j.quascirev.2006.08.008.

Hammer, O., Harper, D., Ryan, P., 2001. PAST: paleontological statistics software package for education and data analysis. Palaeontol. Electron. 4, 1–9.

Harenda, K., Lamentowicz, M., Samson, M., Chojnicki, B.H., 2018. The role of peatlands and their carbon storage function in the context of climate change. In: Zielinski, T., Świątek, B., Kalbarczyk, M. (Eds.), Interdisciplinary Approaches for Sustainable Development Goals. Springer, pp. 169–187. https://doi.org/10.1007/978-3-319-71788-3_12.

Hemming, S.R., 2004. Heinrich events: massive late Pleistocene detritus layers of the North Atlantic and their global climate imprint. Rev. Geophys. 42, RG1005. https://doi.org/10.1029/2003RG000128.

Hu, Y., Jin, Z., Hu, Q., Hu, J., Ni, C., Li, F., 2020. Using stable isotopes to identify nitrogen transformations and estimate denitrification in a semi-constructed wetland. Sci. Total Environ. 720, 137628. https://doi.org/10.1016/j.scitotenv.2020.137628.

Joosten, H., Clarke, D., 2002. Wise Use of Mires and Peatlands: Background and Principles Including a Framework. IMCG/IPS, Finland.

Joosten, H., Convention on Wetlands, 2021. Global guidelines for Peatland Rewetting and Restoration. Ramsar Technical Report No. 11. Secretariat of the Convention on Wetlands, Gland, Switzerland.

Kendall, C., Elliott, E.M., Wankel, S.D., 2008. Tracing anthropogenic inputs of nitrogen to ecosystems. Chapter 12. In: Michener, Robert, Lajtha, Kate (Eds.), Stable Isotopes in Ecology and Environmental Science, pp. 375–449. https://doi.org/10.1002/9780470691854.ch12.

Kohn, M.J., 2010. Carbon isotope compositions of terrestrial C_3 plants as indicators of (paleo)ecology and (paleo)climate. Proc. Natl. Acad. Sci. 107, 19691–19695. https://doi.org/10.1073/pnas.1004933107.

Krammer, K., Lange-Bertalot, H., 1999a. Bacillariophyceae 1 Teil: Naviculaceae Süβwasserflora von Mitteleuropa Freshwater Flora of Central Europe Band 2/1. Spektrum Akademischer Verlag, Heidelberg.

Krammer, K., Lange-Bertalot, H., 1999b. Bacillariophyceae 2 Teil: Bacillariaceae, Epithemiaceae, Surirellaceae Süβwasserflora von Mitteleuropa Band 2/2. Elsevier Spektrum Akademischer Verlag, München.

Krammer, K., Lange-Bertalot, H., 2004a. Bacillariophyceae 3 Teil: Centrales, Fragilariaceae, Eunotiaceae Süβwasserflora von Mitteleuropa Band 2/3 Spektrum. Akademischer Verlag, Heidelberg.

Krammer, K., Lange-Bertalot, H., 2004b. Bacillariophyceae 4 Teil: Achnanthaceae, Kritische Ergänzungen zu Achnanthes, Navicula, Gomphonema Süβwasserflora von Mitteleuropa Band 2/4. Spektrum Akademischer Verlag, Heidelberg.

Ku, H.W., Chen, Y.G., Chan, P.S., Liu, H.C., Lin, C.C., 2007. Paleo-environmental evolution as revealed by analysis of organic carbon and nitrogen: a case of coastal Taipei Basin in Northern Taiwan. Geochem. J. 41, 111–120. https://doi.org/10.2343/geochemj.41.111.

Lähteenoja, O., Reátegui, Y.R., Räsänen, M., Torres, D.D.C., Oinonen, M., Page, S., 2012. The large Amazonian peatland carbon sink in the subsiding Pastaza-Marañón

foreland basin, Peru. Glob. Chang. Biol. 18, 164–178. https://doi.org/10.1111/j.1365-2486.2011.02504.x.7.
Legendre, P., Legendre, L., 2012. Numerical Ecology, 3rd English edition. Elsevier.
Loisel, J., Yu, Z., Beilman, D.W., Camill, P., Alm, J., Amesbury, M.J., Anderson, D., Andersson, S., Bochicchio, C., Barber, K., Belyea, L.R., Bunbury, J., Chambers, F.M., Charman, D.J., De Vleeschouwer, F., Fiałkiewicz-Kozieł, B., Finkelstein, S.A., Gałka, M., Garneau, M., Hammarlund, D., Hinchcliffe, W., Holmquist, J., Hughes, P., Jones, M.C., Klein, E.S., Kokfelt, U., Korhola, A., Kuhry, P., Lamarre, A., Lamentowicz, M., Large, D., Lavoie, M., MacDonald, G., Magnan, G., Mäkilä, M., Mallon, G., Mathijssen, P., Mauquoy, D., McCarroll, J., Moore, T.R., Nichols, J., O'Reilly, B., Oksanen, P., Packalen, M., Peteet, D., Richard, P.J., Robinson, S., Ronkainen, T., Rundgren, M., Sannel, A.B.K., Tarnocai, C., Thom, T., Tuittila, E.-S., Turetsky, M., Väliranta, M., van der Linden, M., van Geel, B., van Bellen, S., Vitt, D., Zhao, Y., Zhou, W., 2014. A database and synthesis of northern peatland soil properties and Holocene carbon and nitrogen accumulation. Holocene 24, 1028–1042. https://doi.org/10.1177/0959683614538073, 2014.
Loisel, J., van Bellen, S., Pelletier, L., Talbot, J., Hugelius, G., 2017. Insights and issues with estimating northern peatland carbon stocks and fluxes since the last glacial maximum. Earth Sci. Rev. 165, 59–80. https://doi.org/10.1016/j.earscirev.2016.12.001.
Longman, J., Veres, D., Finsinger, W., Heiri, O., Hubay, K., Hutchinson, S.M., LeRuez, D., Persoiu, A., Tămaş, T., 2021. Extremely high long-term carbon accumulation rates from mountainous peatlands in Central–Eastern Europe. Clim. Past 17, 2633–2651. https://doi.org/10.5194/cp-17-2633-2021.
López-Sáez, J.A., Carrasco, R.M., Turu, V., Ruiz-Zapata, B., Gil-García, M.J., Luelmo-Lautenschlaeger, R., Pérez-Díaz, S., Alba-Sánchez, F., Abel-Schaad, D., Ros, X., Pedraza, J., 2020. Late glacial-early Holocene vegetation and environmental changes in the Western Iberian central system inferred from a key site: the Navamuño record, Béjar range (Spain). Quat. Sci. Rev. 230, 106167. https://doi.org/10.1016/j.quascirev.2020.106167.
Lourenco, M., Fitchett, J.M., Woodborne, S., 2023. Peat definitions: a critical review. Prog. Phys. Geogr. Earth Environ. 47, 506–520. https://doi.org/10.1177/03091333221118353.
Meyers, P.A., 1994. Preservation of elemental and isotopic source identification of sedimentary organic matter. Chem. Geol. 114, 289–302. https://doi.org/10.1016/0009-2541(94)90059-0.
Meyers, P.A., 2003. Applications of organic geochemistry to paleolimnological reconstructions: a summary of examples from the Laurentian Great lakes. Org. Geochem. 34, 261–289. https://doi.org/10.1016/S0146-6380(02)00168-7.
Monnin, E., Indermühle, A., Dällenbach, A., Flückiger, J., Stauffer, B., Stocker, T.F., Raynaud, D., Barnola, J.M., 2001. Atmospheric CO_2 concentrations over the last glacial termination. Science 291, 112–114. https://doi.org/10.1126/science.291.5501.112.
Mooney, S., Tinner, W., 2010. The analysis of charcoal in peat and organic sediments. Mires Peat. 7, 1–18.
Morris, P.J., Swindles, G.T., Valdes, P.J., Ivanovic, R.F., Gregoire, L.J., Smith, M.W., Tarasov, L., Haywood, A.M., Bacon, K.L., 2018. Global peatland initiation driven by regionally asynchronous warming. Proc. Natl. Acad. Sci. USA 115, 4851–4856. https://doi.org/10.1073/pnas.1717838115.
Naughton, F., Goñi, M.F.S., Kageyama, M., Bard, E., Duprat, J., Cortijo, E., Desprat, S., Malaizé, B., Joly, C., Rostek, F., Turon, J.L., 2009. Wet to dry climatic trend in North-Western Iberia within Heinrich events. Earth Planet. Sci. Lett. 284, 329–342. https://doi.org/10.1016/j.epsl.2009.05.001.
Naughton, F., Goñi, M.F.S., Rodrigues, T., Salgueiro, E., Costas, S., Desprat, S., Duprat, J., Michel, E., Rossignol, L., Zaragosi, S., Voelker, A.H.L., Abrantes, F., 2016. Climate variability across the last deglaciation in NW Iberia and its margin. Quat. Int. 414, 9–22. https://doi.org/10.1016/j.quaint.2015.08.073.
Naughton, F., Goñi, M.F.S., Toucanne, S., 2023. Quaternary climate variability and periglacial dynamics. In: Oliva, M., Nývlt, D., Fernández-Fernández, J.M. (Eds.), Periglacial Landscapes of Europe. Springer International Publishing, Cham, pp. 7–35.
Oliva, M., Palacios, D., Fernández-Fernández, J.M., Rodríguez-Rodríguez, L., García-Ruiz, J.M., Andrés, N., Carrasco, R.M., Pedraza, J., Pérez-Alberti, A., Valcárcel, M., Hughes, P.D., 2019. Late quaternary glacial phases in the Iberian Peninsula. Earth Sci. Rev. 192, 564–600. https://doi.org/10.1016/j.earscirev.2019.03.015.
Pontevedra-Pombal, X., Castro, D., Carballeira, R., Souto, M., López-Sáez, J.A., Pérez-Díaz, S., Fraga, M., Valcárcel, M., García-Rodeja, E., 2017. Iberian acid peatlands: types, origin and general trends of development. Mires Peat. 19, 1–19. https://doi.org/10.19189/MaP.2016.OMB.260.
Poto, L., Gabrieli, J., Crowhurst, S.J., Appleby, P.G., Ferretti, P., Surian, N., Cozzi, G., Zaccone, C., Turetta, C., Pini, R., Kehrwald, N., Barbante, C., 2013. The first continuous late glacial – Holocene peat bog multi-proxy record from the Dolomites (NE Italian Alps). Quat. Int. 306, 71–79. https://doi.org/10.1016/j.quaint.2013.05.001.
Pu, Y., Meyers, P.A., Werne, J.P., Zhang, H., 2023. The paleolacustrine significance of sedimentary nitrogen isotopes: a comparative study of late Holocene records in two lakes on the Eastern Qinghai-Tibet Plateau. Sci. Total Environ. 893, 164641. https://doi.org/10.1016/j.scitotenv.2023.164641.
Ramsar, 2021. The Convention on Wetlands. Restoring Drained Peatlands: A Necessary Step to Achieve Global Climate Goals. https://www.ramsar.org/sites/default/files/documents/library/rpb5_restoring_drained_peatlands_e.pdf.
Rasmussen Clausen, H.B., Cvijanovic, I., Dahl-Jensen, D., Johnsen, S.J., Fischer, H., Gkinis, V., Guillevic, M., Hoek, W.Z., Lowe, J.J., Pedro, J.B., Popp, T., Seierstad, I.K., Steffensen, J.P., Svensson, A.M., Vallelonga, P., Vinther, B.M., Walker, M.J.C., Wheatley, J.J., Winstrup, M., 2014. A stratigraphic framework for abrupt climatic changes during the last glacial period based on three synchronized Greenland ice-core records: refining and extending the INTIMATE event stratigraphy. Quat. Sci. Rev. 106, 14–28. https://doi.org/10.1016/j.quascirev.2014.09.007., S.O., Bigler, M., Blockley, S.P., Blunier, T., Buchardt, S.L.
Rasmussen, S.O., Vinther, B.M., Clausen, H.B., Andersen, K.K., 2007. Early Holocene climate oscillations recorded in three Greenland ice cores. Quat. Sci. Rev. 26, 1907–1914. https://doi.org/10.1016/j.quascirev.2007.06.015.
Reille, M., Lowe, J.J., 1993. A re-evaluation of the vegetation history of the Eastern Pyrenees (France) from the end of the last glacial to the present. Quat. Sci. Rev. 12, 47–77. https://doi.org/10.1016/0277-3791(93)90048-Q.
Reimer, P.J., Austin, W.E.N., Bard, E., Bayliss, A., Blackwell, P.G., Ramsey, C.B., Butzin, M., Cheng, H., Edwards, R.L., Friedrich, M., et al., 2020. The IntCal20 Northern Hemisphere radiocarbon age calibration curve (0–55 cal kBP). Radiocarbon 62, 725–757.
Reixach, T., Delmas, M., Braucher, R., Gunnell, Y., Mahé, C., Calvet, M., 2021. Climatic conditions between 19 and 12 ka in the Eastern Pyrenees, and wider implications for atmospheric circulation patterns in Europe. Quat. Sci. Rev. 260, 106923. https://doi.org/10.1016/j.quascirev.2021.106923.
Rivera-Rondón, C.A., Catalan, J., 2017. The ratio between chrysophycean cysts and diatoms in temperate, mountain lakes: some recommendations for its use in paleolimnology. J. Paleolimnol. 57, 273–285. https://doi.org/10.1007/s10933-017-9946-2.
Rull, V., Blasco, A., Calero, M., Blaauw, M., Vegas-Vilarrúbia, T., 2023. A continuous centennial late glacial-early Holocene (15-10 cal kyr BP) palynological record from the Iberian Pyrenees and regional comparisons. Plants (Basel) 12, 3644. https://doi.org/10.3390/plants12203644.
Ruppel, M., Väliranta, M., Virtanen, T., Korhola, A., 2013. Postglacial spatiotemporal peatland initiation and lateral expansion dynamics in North America and northern Europe. The Holocene 23, 1596–1606. https://doi.org/10.1177/09596836134990.
Sierro, F.J., Hodell, D.A., Curtis, J.H., Flores, J.A., Reguera, I., Colmenero-Hidalgo, E., Bárcena, M.A., Grimalt, J.O., Cacho, I., Frigola, J., Canals, M., 2005. Impact of iceberg melting on Mediterranean thermohaline circulation during Heinrich events. Paleoceanography 20, PA2019. https://doi.org/10.1029/2004PA001051.
Tanneberger, F., Tegetmeyer, C., Busse, S., Barthelmes, A., Shumka, S., et al., 2017. The peatland map of Europe. Mires and Peat 19, 1–17.
Thornton, S.F., McManus, J., 1994. Application of organic carbon and nitrogen stable isotope and C/N ratios as source indicators of organic matter provenance in estuarine systems: evidence from the Tay Estuary, Scotland. Estuar. Coast. Shelf Sci. 38, 219–233. https://doi.org/10.1006/ecss.1994.1015.
Tolonen, K., Turunen, J., 2006. Accumulation rates of carbon in mires in Finland and implications for climate change. Holocene 6, 171–178. https://doi.org/10.1177/095968369600600204.
Treat, C.C., Kleinen, T., Broothaerts, N., Dalton, A.S., Dommain, R., Douglas, T.A., Drexler, J.Z., Finkelstein, S.A., Grosse, G., Hope, G., Hutchings, J., Jones, M.C., Kuhry, P., Lacourse, T., Lähteenoja, O., Loisel, J., Notebaert, B., Payne, R.J., Peteet, D.M., Sannel, A.B.K., Stelling, J.M., Strauss, J., Swindles, G.T., Talbot, J., Tarnocai, C., Verstraeten, G., Williams, C.J., Xia, Z., Yu, Z., Väliranta, M., Hättestrand, M., Alexanderson, H., Brovkin, V., 2019. Widespread global peatland establishment and persistence over the last 130,000 y. Proc. Natl. Acad. Sci. USA 116, 4822–4827. https://doi.org/10.1073/pnas.1813305116.
Turney, C.S.M., Wheeler, D., Chivas, A.R., 2006. Carbon isotope fractionation in wood during carbonization. Geochim. Cosmochim. Acta 70, 960–964. https://doi.org/10.1016/j.gca.2005.10.031.
Turu, V., Carrasco, R.M., Pedraza, J., Ros, X., Ruiz-Zapata, B., Soriano-López, J.M., Mur-Cacuho, E., Pélachs-Mañosa, A., Muñoz-Martín, A., Sánchez, J., Echeverria-Moreno, A., 2018. Late glacial and post-glacial deposits of the Navamuño peatbog (Iberian Central System): chronology and paleoenvironmental implications. Quat. Int. 470, 82–95. https://doi.org/10.1016/j.quaint.2017.08.018.
United Nations Environmental Programme, 2022. Global Peatlands Assessment – The State of the World's Peatlands: Evidence for Action toward the Conservation, Restoration, and Sustainable Management of Peatlands. Main Report. Global Peatlands Initiative. United Nations Environment Programme, Nairobi.
Van Dam, H., Mertens, A., Sinkeldam, J., 1994. A coded checklist and ecological indicator values of freshwater diatoms from the Netherlands. Neth. J. Aquat. Ecol. 28, 117–133. https://doi.org/10.1007/BF02334251.
Vegas-Vilarrúbia, T., Blasco, A., Calero, M.Á., Blaauw, M., Garcés, S., Buchaca, T., Cañellas, N., Rull, V., 2024. Lakes as Sentinels of Global Change in the Aigüestortes i Estany de Sant Maurici National Park: A Multidisciplinary Analysis of the Late Glacial and Holocene Periods. Monography of the Autonomous Organization of National Parks, Research Program of the National Parks Network (accepted).
Ventura, J., Turu, V., 2022. The glaciers of the Central-Eastern Pyrenees. In: Oliva, M., Palacios, D., Fernández-Fernández, J.M. (Eds.), Iberia, Land of Glaciers. Elsevier, Amsterdam, pp. 87–121.
Montanarella, L., Jones, R.J.A., Hiederer, R., 2004. Distribution of peat and peaty-topped soils in Europe. JRC Publication No. JRC28121. Retrieved from. https://publications.jrc.ec.europa.eu/repository/handle/JRC28121.
Wetlands International. 2025 (n.d.). Peatlands and Climate Change. Retrieved from https://www.wetlands.org/casestudy/peatlands-and-climate-change/.
Wu, H., Zhang, H., Chang, F., Duan, L., Zhang, X., Peng, W., Liu, Q., Zhang, Y., Liu, F., 2021. Isotopic constraints on sources of organic matter and environmental change in Lake Yangzong, Southwest China. J. Asian Earth Sci. 217, 104845.
Yu, Z., Loisel, J., Brosseau, D.P., Beilman, D.W., Hunt, S.J., 2010. Global peatland dynamics since the last glacial maximum. Geophys. Res. Lett. 37, L13402. https://doi.org/10.1029/2010GL043584.
Zeng, N., 2003. Glacial-interglacial atmospheric CO_2 change —the glacial burial hypothesis. Adv. Atmos. Sci. 20, 677–693. https://doi.org/10.1007/BF02915395.

Zeng, N., 2005. Is glacial burial carbon the missing link in the glacial-interglacial atmospheric CO_2 changes. Geophys. Res. Abstr. 7, 03786.
Zeng, N., 2006. Quasi-100 ky glacial-interglacial cycles triggered by subglacial burial carbon release. Clim. Past Discuss. 2, 371–397.
Zollinger, B., Alewell, C., Kneisel, C., Meusburger, K., Gärtner, H., Brandová, D., Ivy-Ochs, S., Schmidt, M.W.I., Egli, M., 2013. Effect of permafrost on the formation of soil organic carbon pools and their physical–chemical properties in the Eastern Swiss Alps. Catena 110, 70–85. https://doi.org/10.1016/j.catena.2013.06.010.